The International Journal of Advanced Manufacturing Technology
https://doi.org/10.1007/s00170-021-06920-y

ORIGINAL ARTICLE

Optimization of internal burnishing operation for energy efficiency, machined quality, and noise emission

Trung-Thanh Nguyen[1] · Minh-Thai Le[2]

Received: 17 December 2020 / Accepted: 15 March 2021
© The Author(s), under exclusive licence to Springer-Verlag London Ltd., part of Springer Nature 2021

Abstract
Boosting energy efficiency and machining quality are prominent solutions to achieve sustainable production for burnishing operations. In this work, an effective optimization has been performed to enhance the energy efficiency (EF_b) and decrease the machining noise (MN) as well as surface roughness (SR) of the internal burnishing operation. The burnishing factors are the spindle speed (S), burnishing feed (f), burnishing depth (D), and the number of rollers (N). The burnishing trails of the hardened material labeled SCr440 have been conducted on a CNC milling machine. The adaptive neuro-based-fuzzy inference system (ANFIS) was used to construct the correlations between the process inputs and burnishing responses. The entropy approach is employed to calculate the weight of each technical objective. The non-dominated sorting particle swarm optimization (NSPSO) is utilized to determine the optimal parameters. A comprehensive model of the production cost is developed to check the effectiveness of the proposed approach. The scientific outcomes revealed that the optimal values of the S, f, D, and N are 1645 RPM, 260 mm/min, 0.08 mm, and 4, respectively. The improvements in the EF_b, SR, and MN are 6.98%, 25.00%, and 2.23%, as compared to the initial values. The machining cost is saved by 6.2% at the optimal solution. Moreover, the scientific finding is a potent technical solution to enhance machining performances for the burnishing process of various components having internal holes.

Keywords Internal burnishing · Energy efficiency · Machining noise · Surface roughness · Entropy

1 Introduction

The burnishing process is a finishing machining approach, which was widely applied to enhance the surface properties of machined components through the application of the burnishing force. The burnishing technology provides various advantages, including the low roughness, high hardness, high depth of the affected layer, and high compressive stress, as compared to conventional approaches, such as hard turning, grinding, and honing [1]. Furthermore, the component's functionality has been greatly improved, contributing significantly to increasing strength behavior and abrasion as well as chemical corrosion resistances. Consequently, improving the technological performances of the burnishing process is an urgent demand to enhance the applicability.

Parameter-based optimizations of different burnishing processes have been executed, in which the surface properties, including the roughness properties, hardness criteria, the depth of the affected layers (AL), and the residual stress (RS) are optimizing responses. Cobanoglu and Ozturk explored the effects of the burnishing speed (V), feed rate (f), and burnishing force (F) on the average roughness (AR) and micro-hardness (MH) of the burnished AISI 1040 steel [2]. The results indicated that the AR and MH were improved by 100.0% and 55.5%, as compared to the initial values. A new ball burnishing tool was developed to analyze the impact of the burnishing force on the mechanical behavior and fatigue of the AISI 1010 steel [3]. The outcomes indicated that the ductility of the burnished steel was enhanced by 49.0%, while the fatigue strength did not increase. A novel load cell having a small burnishing tool was developed to perform the burnishing process on the STAVAX steel [4]. Process parameters were the V, F, lubricant (L), step-over (SO), and the number of passes (NP), while the average roughness (AR) and surface hardness (SH) were objectives.

✉ Minh-Thai Le
thaileminh@lqdtu.edu.vn

[1] Faculty of Mechanical Engineering, Le Quy Don Technical University, 236 Hoang Quoc Viet, Hanoi 100000, Vietnam

[2] Faculty of Special Equipments, Le Quy Don Technical University, 236 Hoang Quoc Viet, Hanoi 100000, Vietnam

Published online: 06 April 2021

The authors stated that the AR was decreased by 91.0% and the SH was enhanced by 8.0% at the optimal point, respectively. The empirical models the AR and MH were proposed in terms of the V, f, and the burnishing depth (D) for the burnishing process of TA2 alloy [5]. The outcomes indicated that the AR was decreased by 63.0% and the MH was enhanced by 28.0%, as compared to the pre-machined surface.

The response surface method (RSM) models of the AR, SH, and profile irregularities (PI) for the burnished aluminum alloy were developed in terms of the V, f, and the depth of penetration (D) [6]. The results exhibited that the enhancements of the AR, PI, and SH were 81.0%, 34.0%, and 17.0% at the optimal solution. The effects of the burnishing strategies on surface integrity have been investigated for the burnished aluminum alloy [7]. The authors concluded that the burnishing crossed path could be effectively used to decrease the roughness, while the successive one was an alternative solution to increase the hardness. The RSM was used to develop empirical models of AR and SH in terms of the F, f, NP, and roller width (RW) for the burnishing process of EN-9 alloy [8]. The findings revealed that the AR was decreased by 94.5% and the SH was increased by 41.7%, respectively. Similarly, the impacts of the processing conditions, such as V, f, and D on the SR, bore size (BS), and ovality (OV) for the internal roller burnishing were presented by John et al. [9]. The results indicated that an accurate hole having low roughness was obtained at the optimal solution. The regression models of the AR and SH for the ultrasonic-assisted burnishing process of the aluminum alloy were developed by Teimouriet et al. [10]. The small deviations between the predictive and experimental results indicated that the proposed models were adequate. A magnet-based ball burnishing tool was developed to improve the tribological properties of the burnished surface [11]. The author stated that the burnished quality was better than the grinding approach. The regression models of the AR, SH, and AL were developed regarding the V, f, and D for the internal burnishing operation of carbon steel [12]. The authors stated that a set of feasible solutions could be employed to enhance surface properties. Moreover, Nguyen and Le optimized the maximum height roughness (R_y), AR, and SH for the burnishing of hardened steel using the Kriging models [13]. The authors stated that the improvements in the R_y, AR, and SH were 96.0%, 92.0%, and 45.0%, respectively. The RSM models of the AR and SH were developed regarding the V, f, and F for the diamond burnishing process of 17-4 PH stainless steel under minimum quantity lubrication (MQL) environment [14]. The results indicated that the optimal values of the AR and SH were 0.07 μm and 363 HV, respectively. The impacts of the V, f, F, and d_b on the AR, SH, RS, and the surface morphology for the cryogenic burnishing of stainless steel 17-4 H were explored by Sachin et al. [15]. The authors stated that the proposed operation was effectively improved surface properties.

To overcome the increase in the energy price, carbon emission, and resource exhaust, environmental metrics have become primary considerations of manufacturers and researchers. For this purpose, energetic criteria, including the burnishing energy (BE), energy consumed (EC), and power factor (PF) of different burnishing processes, were addressed. An adaptive network-based fuzzy inference system was applied to decrease the burnishing energy as well as AR and improve the SH for the ultrasonic-assisted burnishing process of AA6061-T6 alloy [16]. The optimal values of the BE, AR, and SH were 1.4 kJ, 0.72 μm, and 156 HV, respectively. The impacts of the V, f, and D on the EC, SR, HA, and PF for the flat burnishing operation of the die steel were explored by Nguyen et al. [17]. The authors stated that the improvements in the EC, AR, SH, and the PF were 49.5%, 13.8%, 21.8%, and 56.0%, respectively. The Kriging models of the EC, SH, and mean roughness square (R_z) for the burnishing process were developed by Nguyen et al. [18]. The findings indicated that the EC and R_z were decreased by 39.5% and 7.8%, respectively, while the SH was increased by 29.6%. Similarly, the improved Kriging models of the EC, AR, and Vicker hardness (VH) of the burnished aluminum alloy 6061 were proposed by Nguyen et al. [19]. The authors stated that the EC and AR were decreased by 20.15% and 65.38%, respectively, while the VH was improved by 30.05%.

As a result, different investigations have been performed to analyze the burnishing process's behaviors using experimental, numerical, and analytical techniques. The common inputs are the spindle speed (burnishing speed), feed rate, burnishing depth, burnishing force, pressure, step-over, the number of passes, and lubricant conditions, while the regular objectives are the roughness properties, hardness criteria, the depth of the affected layer, compressive stress, energy consumed, energy efficiency, and power factor. Besides, various optimization approaches have been employed to render the correlations and obtain optimal values. Unfortunately, the deficiencies of published works for different burnishing processes can be listed as follows:

Most of the previous investigations focus on optimizations of technical performances for the flat and external cylindrical burnishing operations. However, the influences of machining parameters on the energy efficiency and the machining noise for the internal burnishing operation have not been analyzed. To decrease environmental impacts and obtain sustainable manufacturing, the energy efficiency and machining noise of the burnishing process should be minimized (Fig. 1).

The comprehensive model of the energy efficiency and machining noise in terms of process parameters for the internal burnishing process has not been developed. It is necessary to develop predictive models under a variety of machining parameters, which can be used for prediction purposes.

The selection of optimal parameters to solve the trade-off between the energy efficiency, machining noise, and the

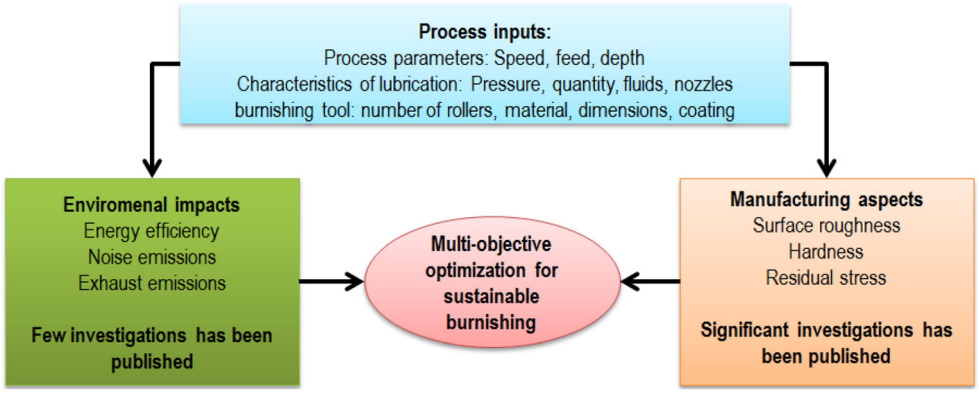

Fig. 1 The sustainable approach for the burnishing operation

surface roughness for the internal roller burnishing operation has not been presented.

To bridge these analyzed research gaps, a parameter-based optimization of the burnishing operation has been addressed to improve the energy efficiency (EF_b) and decrease the machining noise (MN) as well as average roughness (AR). The industrial steel labeled SCr440 is extensively employed to produce military components having deep holes and high-pressure bushings. The predictive models of the machining responses are proposed using the adaptive neuro-based fuzzy inference system and experimental data. The entropy approach was employed to determine the weight values of machining objectives. The optimal factors are determined with the support of the non-dominated sorting particle swarm optimization.

2 Optimization framework

2.1 Optimization issues

In the current investigation, the environmental impacts (i.e., energy efficiency and noise emissions) and the manufacturing aspect (surface roughness) are simultaneously optimized to obtain sustainable manufacturing.

The typical profile of the power consumption for the burnishing process can be found in Fig. 2. The total power consumed in the burnishing operation is divided into the start-up energy (E_{st}), standby energy (E_{sb}), transition energy for the spindle acceleration/deceleration state (E_{ts}), air-burnishing energy (E_{air}), and energy consumed in the burnishing state (E_b). The energy efficiency of the burnishing process is calculated

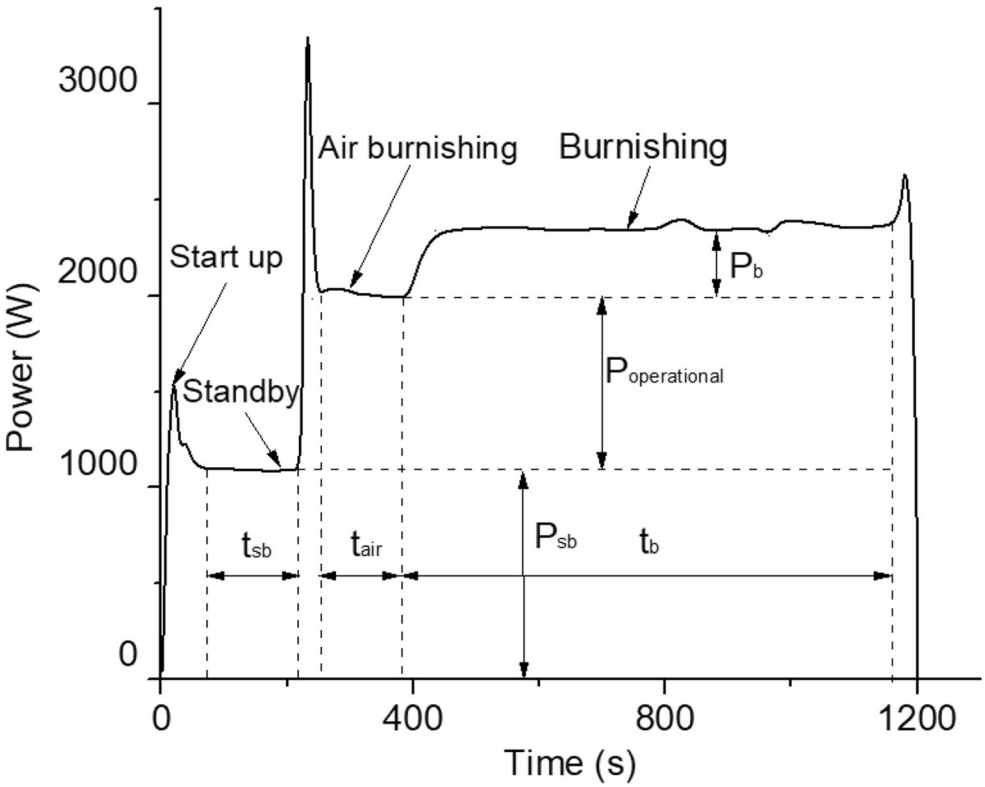

Fig. 2 The typical profile of the power consumption for the burnishing process

Table 1 Parameters for optimization process

Symbol	Parameters	Level 1	Level 2	Level 3
S	Spindle speed (RPM)	1000	1400	1800
f	Burnishing feed (mm/min)	250	400	550
D	Burnishing depth (mm)	0.06	0.09	0.12
N	Number of roller	2	3	4

as the ratio of the burnishing energy (E_b) and the total energy consumed by the machine tool (E_M), which is expressed as:

$$EF_b = \frac{E_b}{E_M} = \frac{P_b \times t_b}{P_M \times t_b} = \frac{P_b}{P_{sb} + P\text{operational} + Pb} \quad (1)$$

where P_b-the burnishing power; P_M-the total power consumed by the machine used; t_b-the burnishing time.

The surface roughness (SR) is computed as:

$$SR = \frac{\sum_{1}^{n} R_{ai}}{n} \quad (2)$$

where R_{ai}, the arithmetic roughness after the burnishing operation at the measured position; n, the number of measured points.

The machining noise (MN) is calculated as:

$$MN = \frac{\sum_{i=1}^{n} MN_i}{n} \quad (3)$$

where MN_i, the machining noise at the i_{th} time measured; n, the number of measured points.

For the burnishing process, affecting factors are process parameters (burnishing speed, feed rate, and burnishing depth), the characteristics of lubrication (pressure, quantity, kinds of the fluid, number of nozzles), the configuration of the burnishing tool (number of rollers, roller material, roller dimensions, roller materials). Machining factors considered are listed in Table 1. The values of the varied inputs are selected based on the recommendations of the manufacturers for the burnishing, workpiece properties, and characteristics of the machine tool. Consequently, the optimizing issue is represented as:

Find X = [S, f, D, and N]
Maximize EF_b; Minimize SR and MN.
Constraints: $1000 \le S \le 1800$ (RPM); $250 \le f \le 550$ (mm/min); $0.06 \le D \le 0.12$ (mm); $2 \le N \le 4$.

2.2 Optimization approach

The optimization procedure for the internal burnishing process includes the following steps (Fig. 3):

Step 1: A set of burnishing experiments is executed to obtain the experimental data based on parameter combinations [20, 21].

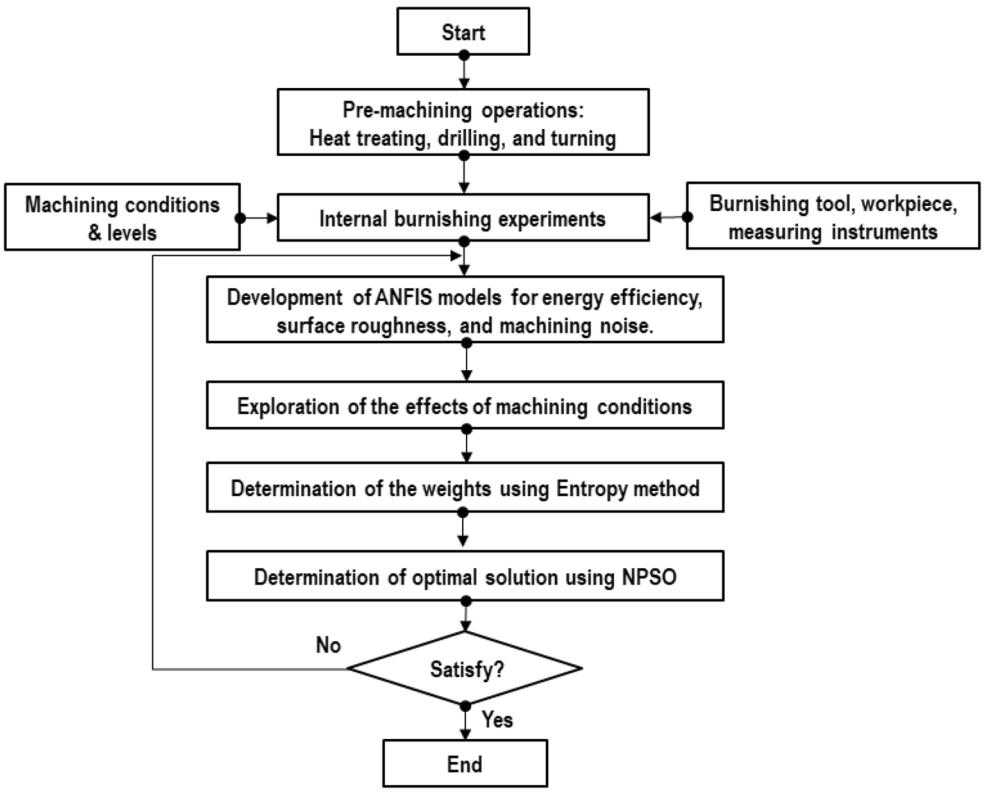

Fig. 3 Optimization approach

Step 2: The ANFIS models of the EF_b, SR, and MN are developed in terms of machining parameters [22, 23].

In this research, the ANFIS approach is used instead of traditional approaches (RSM and regression method) to describe the relationships between the input parameters and energy efficiency, surface roughness, and machining noise.

ANFIS is a combination of the artificial neural network (ANN) and fuzzy interface system (FIS), which takes the best advantages and overcomes the disadvantages in both techniques in terms of numerical and linguistic knowledge. The ANFIS approach is more transparent and causes less memorization errors in comparison with the ANN. This method provides several advantages including adaptation capability, nonlinear ability, and rapid learning capacity. Consequently, ANFIS is widely employed for modeling, controlling, and parameter estimation in complex systems and operations.

Mamdani and Sugeno are two common ANFIS systems. The output membership functions of the Mandani system can be triangular and Gaussian, while the output membership functions of the Sugeno are either linear or constant. In this investigation, the Sugeno based-ANFIS system is employed due to its high computational efficiency and reliability, as compared to the Mamdani system.

The operating parameters of the Sugeno based-ANFIS model are the number and types of input membership functions (triangular, trapezoidal, bell-shaped, Gaussian, and sigmoid), type of output membership functions (constant or linear), optimization methods (hybrid or back-propagation), and the number of epochs. It is necessary to select the optimal combination of the mentioned parameters for increasing the reliability and accuracy of the network. The ANFIS structure using five-layer feed-forward neural networks is depicted in Fig. 3.

The two rules of the ANFIS are stated as:

$$Rule\ 1: If\ x\ is\ A_1\ and\ y\ is\ B_1, then\ f_1 = p_1x + q_1y + r_1 \quad (4)$$

$$Rule\ 2: If\ x\ is\ A_2\ and\ \mathrm{y}\ is\ B_2, then\ f_1 = p_2x + q_2x + r_2 \quad (5)$$

where x and f are input and output. A_i and B_i denote the membership functions of each of the input x and y, respectively. p_i, q_i and r_i are constants.

The designed ANFIS model using five-layer feed forward neural networks for the burnishing responses is expressed as follows (Fig. 4):

Layer 1 (Fuzzification layer): The primary duty of the first layer is to select the membership degrees for each input using the given membership functions (MF). The outputs of this layer are identified as:

$$L_1^i = O_1^i = \mu_{Ai}(x) \quad (6)$$

where x is the input of the i_{th} node. A_i denotes the linguistic label associated with this node function. $\mu_{Ai}(x)$ presents the membership function of A_i. $\mu_{Ai}(x)$ normally is chosen as:

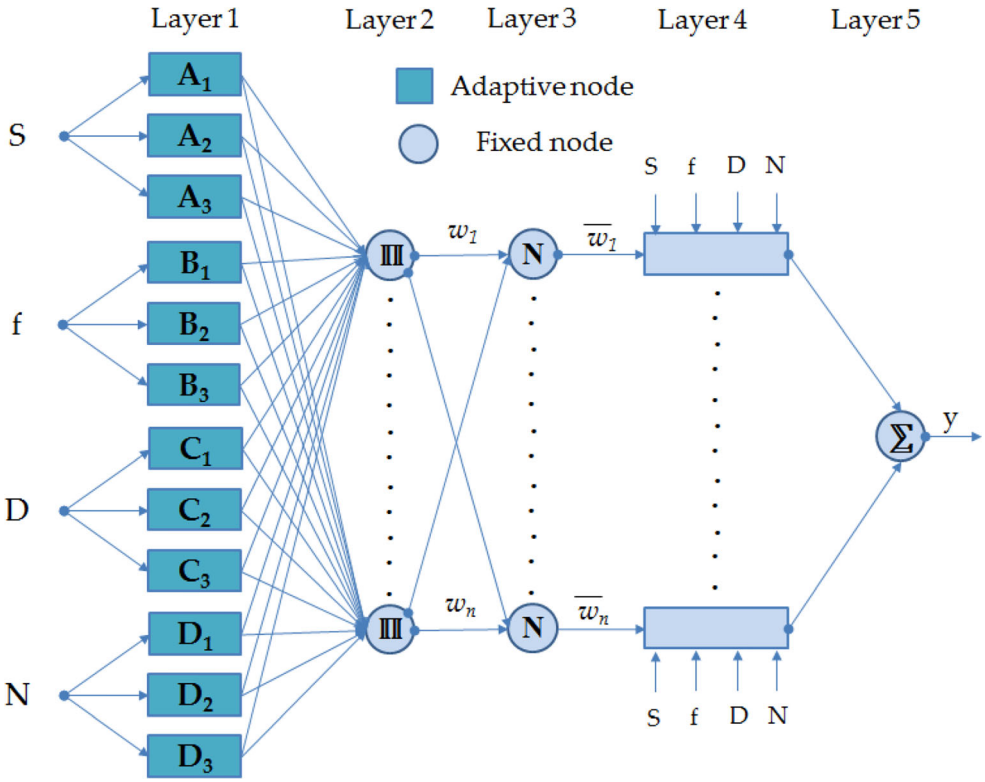

Fig. 4 The typical structure of the ANFIS model

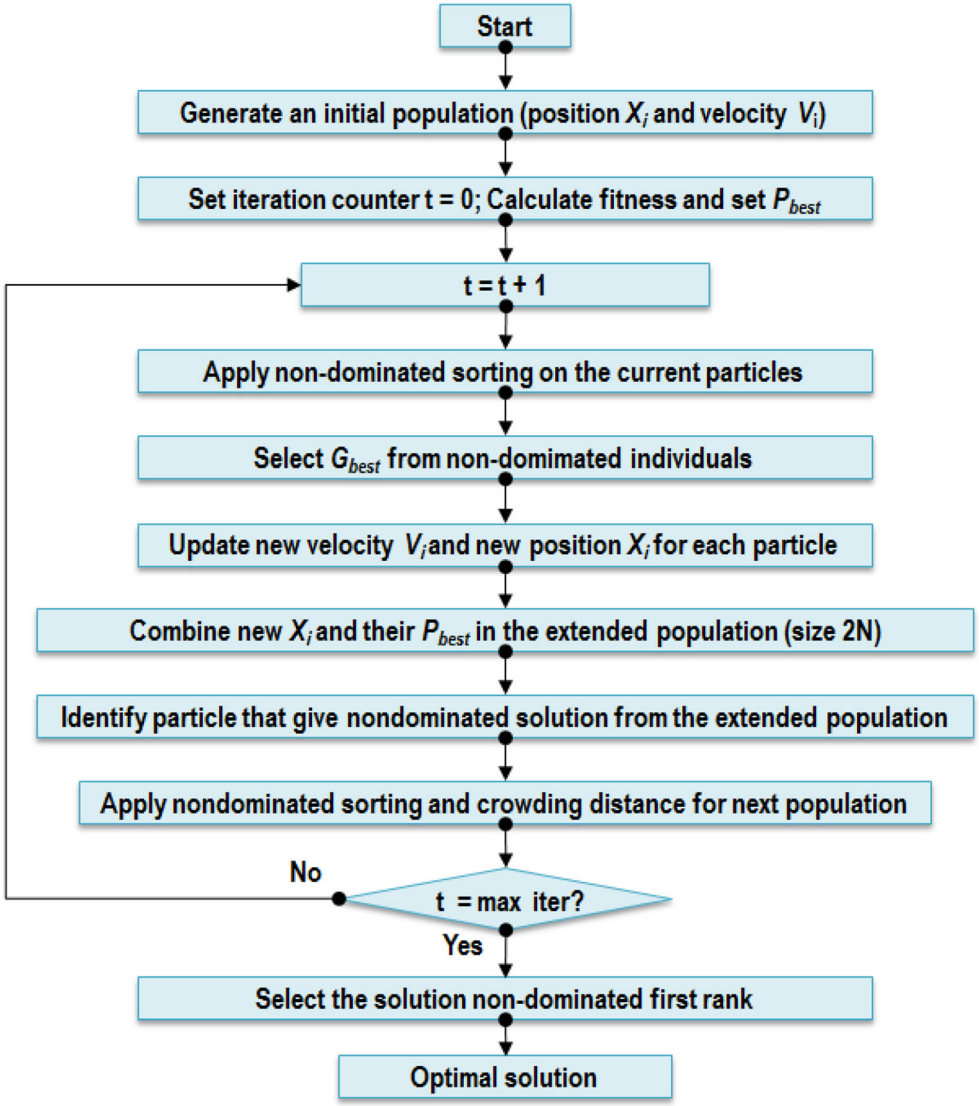

Fig. 5 Operating principle of the NSPSO

$$\mu_{Ai}(x) = \frac{1}{1 + \left[\left(\frac{x-c_i}{2}\right)^2\right]^{b_i}} \tag{7}$$

or

$$\mu_{Ai}(x) = \exp\left\{-\left(\frac{x-c_i}{a_i}\right)^2\right\} \tag{8}$$

where a_i, b_i, and c_i are the premise parameters.

Layer 2 (Rule layer): Every node in this layer is the fixed node labeled Π, which is employed to the firing strength ω_i of a rule. The output of each node is the product of all incoming signals to it and expressed as:

$$L_2^i = \omega_i = \mu_i(x) \times \mu_{B_i}(y), i = 1, 2, 3..., N \tag{9}$$

Layer 3 (Normalized layer): Every node in this layer is the fixed node labeled N. Each i^{th} node calculates the ratio of the i^{th} rule's firing strength to the sum of firing strengths of all the rules. The output presenting the normalized firing strength is represented as:

$$L_3^i = \overline{\omega}_i = \frac{\omega_i}{\sum_{i=1}^{n} \omega_i}, i = 1, 2, 3..., N \tag{10}$$

Layer 4 (Defuzzification layer): Every node in this layer is an adaptive node. The primary duty of the fourth layer is to defuzzificate received inputs and assign the consequent parameters of the rules. The output of this layer is expressed as:

Table 2 Chemical compositions of the 40X

C (%)	Si (%)	Mn (%)	Ni (%)	Cr (%)	Cu (%)	P (%)	S (%)
0.38	0.27	0.6	0.3	0.9	0.3	0.035	0.035

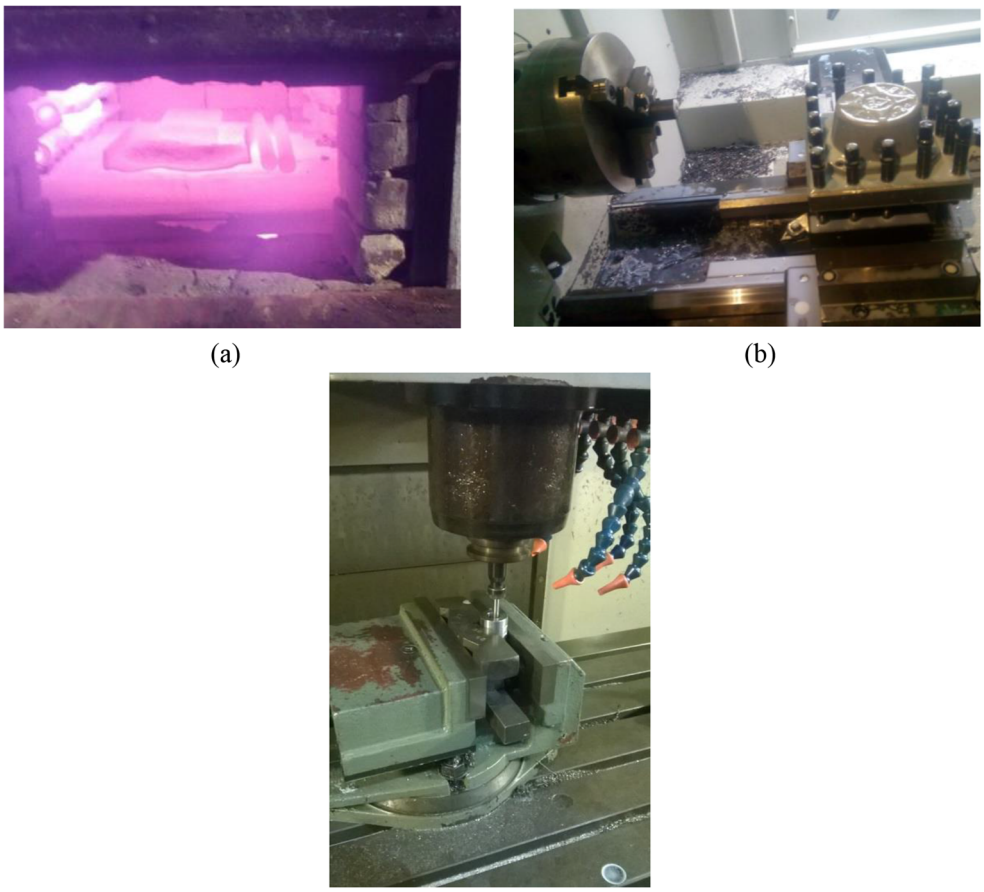

Fig. 6 Experimental procedure. **a** Heat treatment. **b** Drilling and turning. **c** Setting the origin of the workpiece

$$L_4^i = \overline{\omega}_i f_i = \overline{\omega}_i (p_i x + q_i x + r_i), i = 1, 2, 3, \ldots, N \tag{11}$$

where p_i, q_i, and r_i are the consequent parameters, respectively.

Layer 5 (Output layer): This layer comprises of only one fixed node. The primary duty of the fifth layer is to calculate the overall output as the summation of all incoming signals. The output of this layer is expressed as:

$$L_5^i = \sum_i \overline{\omega}_i f_i = \frac{\sum_i \omega_i f_i}{\sum_i \omega_i} \tag{12}$$

Step 3: The weight of each objective is determined using the entropy method.

For higher the better approach, the measured response is calculated as:

$$r_{ij} = \frac{x_{ij}}{\max_j x_{ij}}, (i = 1, \ldots, m; j = 1, \ldots, n) \tag{13}$$

For lower the better approach, the measured response is calculated as:

$$r_{ij} = \frac{\min_j x_{ij}}{\mathrm{x}_{ij}}, (i = 1, \ldots, m; j = 1, \ldots, n) \tag{14}$$

The values of the responses are normalized as:

$$p_{ij} = \frac{r_{ij}}{\sum_{i=1}^{m} r_{ij}}, (i = 1, \ldots, m; j = 1, \ldots, n) \tag{15}$$

where: p_{ij}-the normalized response.

The entropy value E_j of the i_{th} index is calculated as:

$$E_j = -\frac{\sum_{j=1}^{m} p_{ij} \times \ln p_{ij}}{\ln m}, (i = 1, \ldots, m; j = 1, \ldots, n) \tag{16}$$

The entropy weight w_i is calculated as:

$$w_i = \frac{1 - E_j}{\sum_{j=1}^{n} (1 - E_j)} \tag{17}$$

Step 4: Determination of the optimal values of process inputs and outputs using the ANFIS-NSPSO.

The developed ANFIS models are employed to obtain optimal factors using the NOPSO. NSPSO is one of the meta-

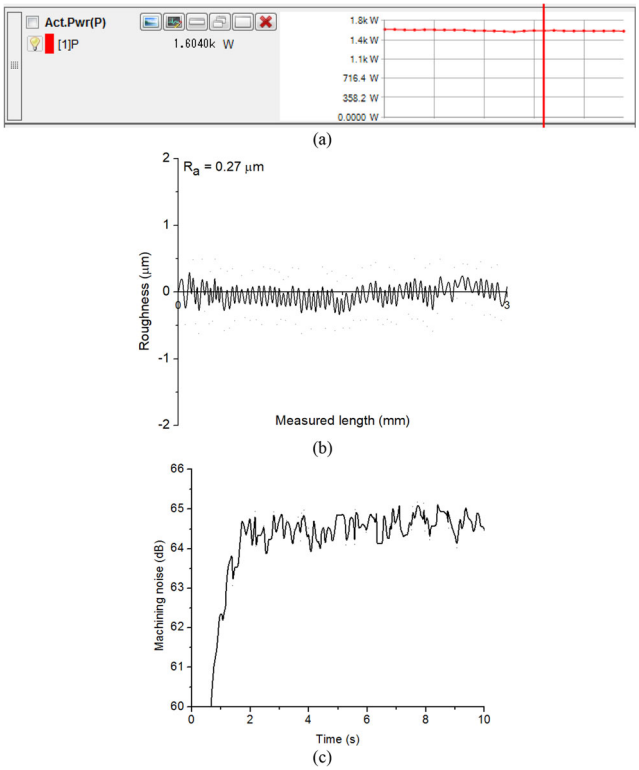

Fig. 7 Representative results at the trail No. 58. **a** Power consumed. **b** Average roughness. **c** Machining noise

heuristic optimization algorithms, which is employed to solve the complex optimizing issue having contradictory objectives [24, 25]. The purpose of the multi-objective hybrid algorithm is to combine the particle swarm optimization (PSO) and the non-dominated sorting genetic algorithm (NSGA-II) to enhance the working performance and generate the reliable Pareto-front. The NOPSO takes the strengths of two optimizing algorithms, including the fast non-dominated sorting approach, crowding distance ranking, elitist strategy, mutation, selection operations, and the particle swarm searching. Figure 5 depicts the operating steps of the hybrid algorithm:

- Generate an initial population (P) and assign the individual velocity for each particle in the design space. Setting the maximum speed ($v_i^{\max}$) for each variable.
- Sort the population based on the non-dominated operation and crowding distance ranking.
- Execute the rank-based selection operator.
- Assign the fitness of each individual to its non-domination level.
- Randomly select one individual as *gbest* from the non-dominated points. Modify each searching point using the following formula and the *gbest*:

$$v_i^{k+1} = k\left[v_i^k + c_1 \times r_1 \times pbest_i - x_i^k\right) + c_2 \times r_2 \times \left(gbest - x_i^k\right)\Big] \tag{18}$$

$$x_i^{k+1} = x_i^k + v_i^{k+1} \tag{19}$$

where v_i^k and x_i^k present the velocity and position at the k generation, respectively. v_i^{k+1} and x_i^{k+1} denote the velocity and position at the $k+1$ generation, respectively. r_1 and r_2 present a random number between (0, 1). c_1 and c_2 are two constant coefficients balancing the influence of the best personal position of the particle $pbest_i$ and the best global position *gbest*.

- Execute mutation operation.
- Generate an extended population of size 2N based on a combination of the offspring and parent population.
- Sort the generated population and fill the new population of size N.
- If the current rank of the new individual P_i^{k+1} is smaller than or equal to the parent in R, replace the $pbest_i$ with the current individual; otherwise, keep the current $pbest_i$.
- Perform the step (2) to (9) until the convergence is obtained.

Step 4: The optimal factors are selected using the response surface method (RSM) and desirability approach (DA).

The mathematical models of EDD responses are developed using the RSM and experimental data. RSM is extensively applied in design optimization because of its simplicity. The quadratic model is the most effective approximation to present the nonlinear data, which can be expressed as:

$$y = \beta_0 + \sum_{i=1}^{m} \beta_1 x_i + \sum_{i=1}^{m} \beta_2 x_i^2 + \sum_{i=1}^{m-1} \sum_{j=i+1}^{m} \beta_3 x_i x_j + \theta \tag{20}$$

where m and θ denote the number of parameters and approximate error, respectively. β_1, β_2, and β_3 present regression coefficients.

The optimal values of the machining parameters are selected using the desirability approach, in which each burnishing response is transformed into the function of the desirability (d_i).

To maximize the objective, the d_i is computed as:

$$d_i = \begin{cases} 0, Y(x)_i \le L(x)_i \\ \left(\dfrac{Y(x)_i - L(x)_i}{H(x)_i - L(x)_i}\right)^w, \\ L(x)_i < Y(x)_i < -H(x)_i \\ 1, \mathrm{Y(x)}_i \ge H(x)_i \end{cases} \tag{21}$$

To minimize the objective, the d_i is computed as:

$$d_i = \begin{cases} 0, Y(x)_i \le L(x)_i \\ \left(\dfrac{H(x)_i - Y(x)_i}{H(x)_i - L(x)_i}\right)^w, \\ L(x)_i < Y(x)_i < -H(x)_i \\ 1, \mathrm{Y(x)}_i \ge H(x)_i \end{cases} \tag{22}$$

Table 3 Experimental data for the internal roller burnishing operation

No.	S (RPM)	f (mm/min)	D (mm)	N	EF_b (%)	SR (μm)	MN (dB)
Experimental data for developing ANFIS model							
1	1000	250	0.06	2	13.24	0.38	55.9
2	1300	350	0.06	2	16.80	0.39	61.3
3	1600	450	0.06	2	20.99	0.49	68.5
4	1300	250	0.08	2	16.13	0.31	61.7
5	1600	350	0.08	2	20.13	0.41	68.2
6	1000	450	0.08	2	19.46	0.42	63.8
7	1600	250	0.10	2	20.23	0.35	68.2
8	1000	350	0.10	2	18.51	0.35	63.0
9	1300	450	0.10	2	22.39	0.38	69.3
10	1800	550	0.08	3	28.16	0.53	81.9
11	1000	250	0.08	3	16.51	0.35	62.5
12	1800	550	0.08	3	28.16	0.53	81.9
13	1000	550	0.10	3	25.76	0.55	74.6
14	1800	250	0.10	3	24.56	0.38	73.9
15	1800	550	0.10	3	30.18	0.55	84.5
16	1800	550	0.06	3	26.58	0.54	78.7
17	1800	250	0.06	3	20.77	0.41	67.7
18	1000	550	0.06	3	22.56	0.54	69.6
19	1600	450	0.10	4	29.34	0.39	81.3
20	1300	350	0.10	4	25.21	0.35	74.5
21	1000	250	0.10	4	21.71	0.39	69.5
22	1300	450	0.06	4	23.50	0.37	72.2
23	1000	350	0.06	4	19.85	0.42	66.5
24	1600	250	0.06	4	22.16	0.27	67.8
25	1000	450	0.08	4	23.72	0.48	73.4
26	1600	350	0.08	4	25.34	0.31	74.6
27	1300	250	0.08	4	21.49	0.28	68.6
28	1800	250	0.12	4	30.92	0.37	79.4
29	1000	350	0.12	4	25.99	0.51	74.5
30	1800	450	0.12	4	33.74	0.49	86.3
31	1000	250	0.06	4	18.00	0.37	63.5
32	1800	350	0.06	4	25.37	0.34	73.4
33	1800	450	0.06	4	27.10	0.38	77.5
34	1800	250	0.12	4	30.92	0.37	79.4
35	1800	350	0.12	4	32.11	0.42	82.5
36	1000	450	0.12	4	28.20	0.57	78.0
37	1600	550	0.06	2	23.72	0.55	72.4
38	1300	250	0.06	2	14.75	0.36	58.8
39	1000	550	0.06	2	21.38	0.53	64.9
40	1300	550	0.12	2	27.45	0.48	74.5
41	1000	250	0.12	2	18.51	0.30	62.6
42	1600	550	0.12	2	29.15	0.53	79.1
43	1000	550	0.12	2	26.36	0.51	70.8
44	1600	250	0.12	2	22.58	0.35	70.1
45	1300	550	0.12	2	27.45	0.48	74.5
46	1000	450	0.12	3	25.16	0.51	72.5
47	1300	350	0.12	3	24.41	0.37	72.2
48	1600	250	0.12	3	25.13	0.35	73.3
49	1300	450	0.12	3	26.60	0.44	75.5
50	1600	350	0.12	3	26.67	0.39	76.0
51	1000	250	0.12	3	20.79	0.37	66.9
52	1600	450	0.06	3	22.64	0.42	71.6
53	1000	350	0.06	3	17.10	0.42	62.2
54	1300	250	0.06	3	16.68	0.32	61.8
55	1600	250	0.10	3	22.62	0.32	71.1
56	1300	350	0.10	3	22.00	0.34	70.2
57	1000	450	0.10	3	22.87	0.46	70.7
58	1300	250	0.08	3	18.23	0.29	64.9
59	1000	350	0.08	3	18.54	0.39	65.1
60	1600	450	0.08	3	24.20	0.41	74.7
61	1000	250	0.06	3	15.04	0.38	59.5

Table 3 (continued)

No.	S (RPM)	f (mm/min)	D (mm)	N	EF_b (%)	SR (μm)	MN (dB)
62	1600	350	0.06	3	20.56	0.38	67.9
63	1300	450	0.06	3	20.82	0.41	68.1
64	1000	550	0.08	4	26.44	0.56	77.7
65	1300	250	0.08	4	21.49	0.28	68.6
66	1600	550	0.08	4	29.47	0.43	83.0
67	1300	550	0.06	4	26.04	0.44	76.7
68	1600	250	0.06	4	22.16	0.27	67.8
69	1000	550	0.06	4	24.90	0.55	74.7
70	1600	550	0.10	4	31.60	0.47	85.8
71	1000	250	0.10	4	21.71	0.39	69.5
72	1300	550	0.10	4	29.71	0.50	82.5
73	1800	450	0.06	2	22.45	0.57	71.7
74	1000	350	0.06	2	15.50	0.41	58.3
75	1800	250	0.06	2	18.61	0.51	65.7
76	1000	450	0.1	2	21.15	0.41	65.9
77	1800	350	0.1	2	23.71	0.47	73.9
78	1800	250	0.1	2	22.08	0.44	71.4
79	1800	450	0.08	2	23.90	0.53	74.6
80	1800	350	0.08	2	21.78	0.49	71.4
81	1000	250	0.08	2	14.55	0.32	58.7
No.	S (RPM)	f (mm/min)	D (mm)	N	EF_b (%)	SR (μm)	MN (dB)
Experimental data for testing accuracy of the ANFIS model							
82	1200	350	0.09	3	20.38	0.34	68.1
83	1300	450	0.09	4	26.13	0.39	76.9
84	1400	350	0.10	3	22.66	0.35	71.3
85	1350	300	0.12	4	27.33	0.36	75.7
86	1700	450	0.06	2	21.69	0.53	70.0
87	1450	500	0.08	3	24.42	0.42	74.7
88	1600	400	0.09	3	24.07	0.38	74.2

To obtain the objective, the d_i is computed as:

$$d_i = \begin{cases} \left(\frac{Y(x)_i - L(x)_i}{T(x)_i - L(x)_i}\right)^{w_1}, \\ L(x)_i < Y(x)_i < T(x)_i \\ \left(\frac{Y(x)_i - H(x)_i}{T(x)_i - H(x)_i}\right)^{w_2}, \\ T(x)_i < Y(x)_i < H(x)_i \\ 0, \text{otherwise} \end{cases} \quad (23)$$

To satisfy the range, the d_i is computed as:

$$d_i = \begin{cases} 1, L(x)_i < Y(x)_i < H(x)_i \\ 0, \text{otherwise} \end{cases} \quad (24)$$

where L_i (x), H_i (x), and T_i (x) are the low, high, and aimed responses, respectively.

The desirability for multi-objective optimization is computed as:

$$D = \left(\prod_{i=1}^{k} d_i^{r_i}\right)^{1/\sum r_i} \quad (25)$$

where k presents the number of burnishing performances.

Step 5: The effectiveness of applied optimizing techniques is compared.

The optimal outcomes of the process parameters and burnishing performances are compared to evaluate the effectiveness of applied optimizing techniques.

3 Experiments and measurements

Each machining specimen of a steel labeled SCr440 is produced from the hardened round billet. The chemical compositions of the SCr440 are listed in Table 2. A high-frequency furnace is used to produce the hardened steel (Fig. 6a). To produce the interior hole in each workpiece, the drilling and rough turning operations are employed (Fig. 6b). The length, internal, and external dimensions of the pre-machined workpiece are 50 mm, 15 mm, and 30 mm, respectively.

A vertical milling machine namely OKK VM-5 II is used to conduct a set of burnishing experiments. The machine tool has the main power of 22.4 kW for the drive motor and a maximum spindle speed of 10000

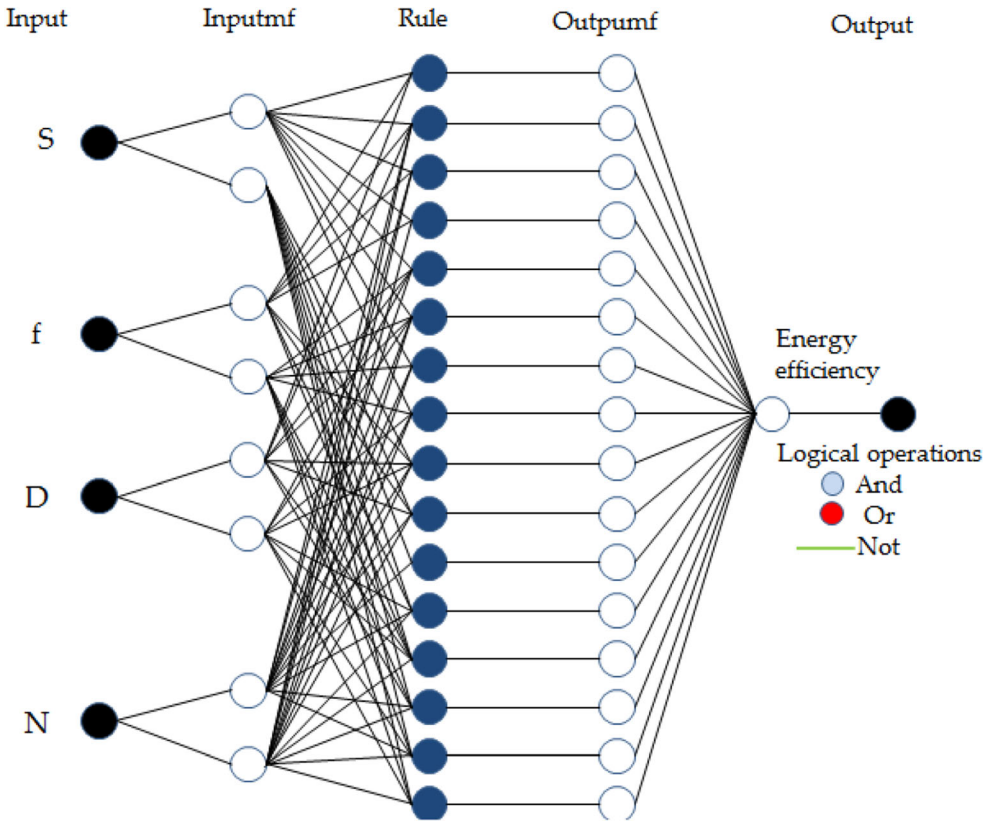

Fig. 8 The 2-2-2-2 structure of ANFIS model for the EF_b

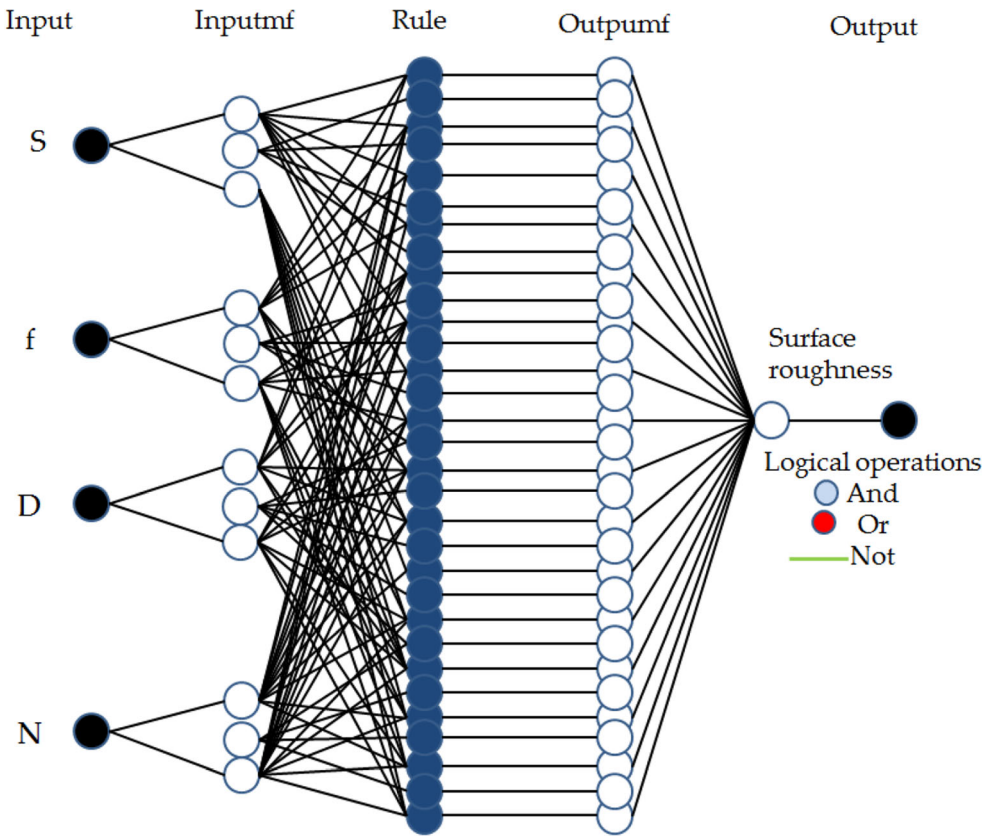

Fig. 9 The 3-3-3-3 structure of ANFIS model for the SR

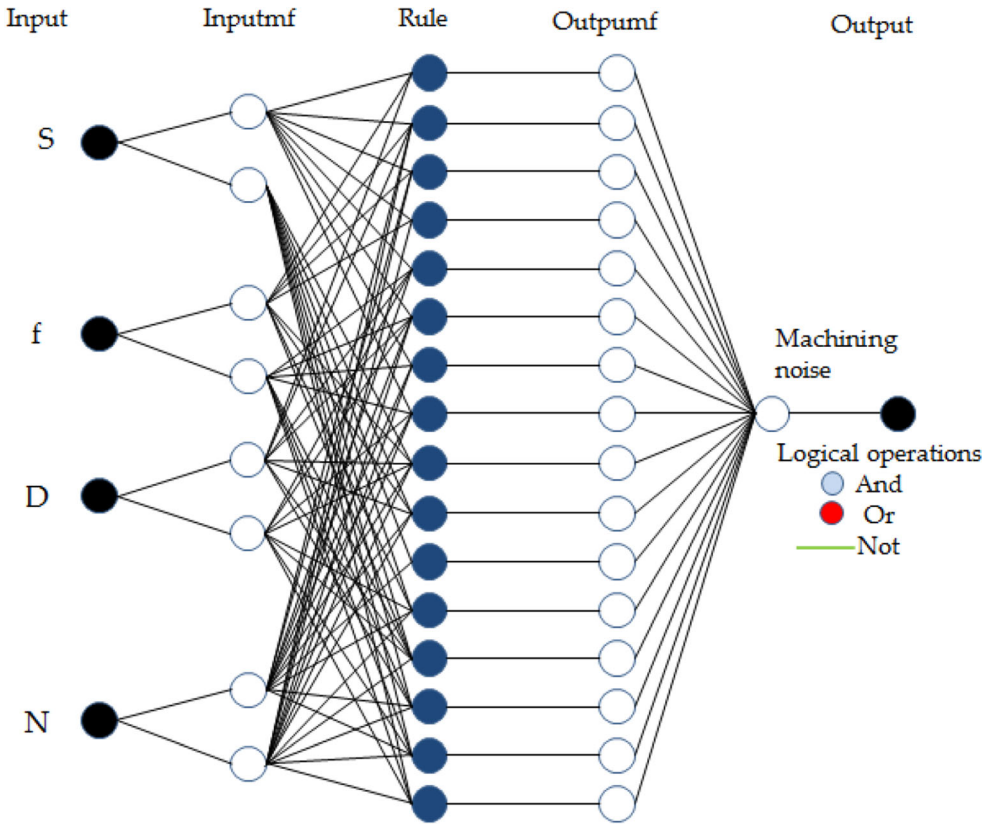

Fig. 10 The 2-2-2-2 structure of ANFIS model for the MN

RPM. The lubrication namely CPC 15A oil is flooded into the burnishing region.

The rotational motion is transferred from the machine spindle to the burnishing tool with the aid of the straight shank (Fig. 6c). The linear motion of the burnishing tool is conducted with the support of the Z-axis. Four hardened rollers can easily be disassembled for different machining purposes.

A power meter (Kyoritsu 6305) is employed to measure the power consumption in the burnishing time based on the connection with the electrical source. The variety of power used of 0.1 s is captured for all experiments. The measured power is represented using commercial software.

The roughness is measured in five different points of the machined surface according to the ISO 4287using a Mitutoyo surftest 301. The measured length of 4 mm is employed for all machining specimens. The measured range of 0.05–40 mm and the resolution of 0.01 mm are employed to enhance accuracy.

A noise meter namely PCE 322A is employed to capture the variety of the real-time noise during burnishing time. The dynamic range of 50 dB and the resolution of 0.1 dB are applied to enhance the accuracy of the measured value. The obtained noise is stored in the memory card and visualized using the commercial software.

The representative results at the experimental No. 58 are shown in Fig. 7.

4 Results and discussions

4.1 Development of ANFIS models

The experimental outcomes of the burnishing operation are shown in Table 3. The obtained data from 1 to 81 are employed to construct the architecture of ANFIS models, while the data from 82 to 88 are used in order to investigate the accuracy of the proposed models.

The 2-2-2-2 structures of the ANFIS models are employed to present the relation between burnishing parameters and the energy efficiency and machining noise (Figs. 8 and 9). The 3-

Table 4 The global errors using different membership functions

ANFIS models	Membership functions		
	gbellmf	*gaussmf*	*gauss2mf*
For the energy efficiency EF_b	0.03284	0.03037	0.03173
For the surface roughness SR	0.00146	0.00095	0.00137
For the machining noise MN	0.02873	0.02484	0.02237

Table 5 The parameters for different ANFIS models

ANFIS models	Number of MFs	Types of output MFs	Optimal method
For the energy efficiency EF_b	2-2-2-2	Linear	Hybrid
For the surface roughness SR	3-3-3-3	Linear	Hybrid
For the machining noise MN	2-2-2-2	Linear	Hybrid

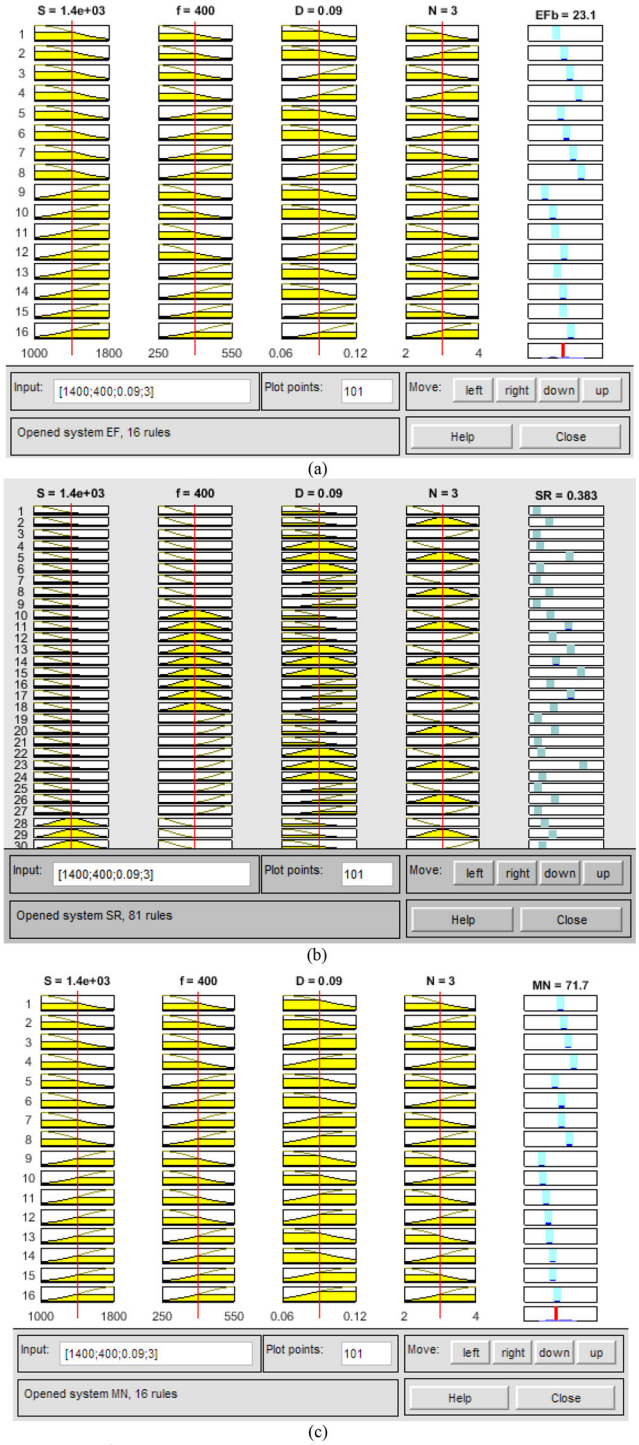

Fig. 11 The rules of ANFIS model for burnishing responses. **a** The rules of ANFIS model for EF_b. **b** The rules of ANFIS model for SR. **c** The rules of ANFIS model for MN

3-3-3 structures of the ANFIS model are used to present the relations between burnishing parameters and the surface roughness (Fig. 10). The global errors of the ANFIS models with different MFs are shown in Table 4. As a result, the membership function labeled *gaussmf* can provide minimal deviations. The operating parameters, including the type of output membership functions, optimization methods, and the number of epochs for three proposed ANFIS models, are shown in Table 5. The rules of ANFIS models for the EF_b, SR, and MN are depicted in Fig. 11 a, b, and c, respectively.

The comparative values between the predicted and experimental values of the EF_b, SR, and MN are shown in Tables 6, 7, and 8, respectively. The small deviations indicated that the ANFIS models can provide acceptable precision.

4.2 ANOVA results for burnishing performances

ANOVA analysis is executed to identify the significance of the ANFIS models and process parameters.

ANOVA results having 95% confidence level for the energy efficiency model are shown in Table 9. The R^2-values of 0.9768 presented that 97.68% of the experimental data are described by the EF_b model. The adjusted R^2 value of 0.9632 showed that 96.32% of the experimental data are described by significant factors. Additionally, the predicted R^2 value of 0.9586 revealed that the EF_b model can be expected to explain 95.86% of the variability in any new data.

The factors having the *p*-value less than 0.05 are considered as significant terms. The meaningful terms are the single factors (*S*, *f*, *D*, and *N*), interactive factors (*Sf*, *SN*, *fN*, and *DN*), and quadratic factors (S^2, f^2, D^2, and N^2). The contributions of the factors considered on the energy efficiency model are depicted in Fig. 12 a. For the single factors, the contributions of the *S*, *f*, *D*, and *N* are 17.40%, 23.14%, 19.01%, and 16.31%. The contributions of the S^2, f^2, D^2, and N^2 are 3.47%, 4.41%, 3.21%, and 3.72%, respectively. For the interactive factors, the contributions of the *Sf*, *SN*, *fN*, and *DN* are 3.19%, 1.14%, 2.31%, and 1.55%, respectively.

ANOVA results having 95% confidence level for the surface roughness model are shown in Table 10. The R^2-values of 0.9787 presented that 97.87% of the experimental data are described by the SR model. The adjusted R^2 value of 0.9676 showed that 96.76% of the experimental data are described by significant factors. Additionally, the predicted R^2 value of

Table 6 Comparative errors for the energy efficiency model

No.	S (RPM)	f (mm/min)	D (mm)	N	EF_b (%)		
					Experiment	ANFIS	Errors (%)
82	1200	350	0.09	3	20.38	20.86	− 2.30
83	1300	450	0.09	4	26.13	26.42	− 1.10
84	1400	350	0.1	3	22.66	22.38	1.25
85	1350	300	0.12	4	27.33	27.59	− 0.94
86	1700	450	0.06	2	21.69	21.36	1.52
87	1450	500	0.08	3	24.42	24.81	− 1.57
88	1600	400	0.09	3	24.07	24.49	− 1.71

0.9612 revealed that the SR model can be expected to explain 96.12% of the variability in any new data.

The factors having the *p*-value less than 0.05 are considered as significant terms. The meaningful terms are the single factors (*S*, *f*, and *N*), interactive factors (*SN* and *DN*), and quadratic factors (S^2, f^2, and D^2). The contributions of the factors considered on the energy efficiency model are depicted in Fig. 12 b. For the single factors, the contributions of the *S*, *f*, and *N* are 13.47%, 48.57%, and 4.53%. The contributions of the S^2, f^2, and D^2 are 18.90%, 1.15%, and 3.58%, respectively. For the interactive factors, the contributions of the *Sf*, *SN*, *fN*, and *DN* are 3.19%, 1.14%, 2.31%, and 1.55%, respectively.

ANOVA results having 95% confidence level for the machining noise model are shown in Table 11. The R^2-values of 0.9734 presented that 97.34% of the experimental data are described by the MN model. The adjusted R^2 value of 0.9652 showed that 96.52% of the experimental data are described by significant factors. Additionally, the predicted R^2 value of 0.9576 revealed that the MN model can be expected to explain 95.76% of the variability in any new data.

The factors having the *p*-value less than 0.05 are considered as significant terms. The meaningful terms are the single factors (*S*, *f*, *D*, and *N*), interactive factors (*Sf, SD, SN, fN,* and *DN*), and quadratic factors (S^2, f^2, and D^2). The contributions of the factors considered on the energy efficiency model are depicted in Fig. 12 c. For the single factor, the contributions of the *S*, *f*, *D*, and *N* are 19.75%, 24.43%, 16.60, and 16.51%. The contributions of the S^2, f^2, and D^2 are 3.51%, 4.49%, and 4.49%, respectively. For the interactive factors, the contributions of the *Sf, SD, SN, fN,* and *DN* are 1.21%, 1.23%, 3.45%, 2.74%, and 1.70%, respectively.

4.3 The impacts of process parameters on the burnishing performances

The impacts of burnishing parameters on energy efficiency are illustrated in Fig. 13.

Figure 13 a presents the influences of the spindle speed and feed rate on energy efficiency. It can be stated that higher energy efficiency is found with an increased spindle speed and/or feed rate. The phenomena can be explained as follows. An increased feed rate causes a higher power consumed of the drive system to satisfy the setting value. The active burnishing power is then increased; hence, energy efficiency is enhanced. When the spindle speed increases, higher burnishing momentum is produced, which requires higher power consumed of the spindle motor. Consequently, higher burnishing power is obtained, which leads to enhanced energy efficiency. Practically, a higher feed rate and/or spindle speed causes faster-burnishing operation due to the reduction in the burnishing time; hence, higher energy efficiency is achieved. Moreover, higher spindle speed causes an increased

Table 7 Comparative errors for the surface roughness model

No.	S (RPM)	f (mm/min)	D (mm)	N	SR (μm)		
					Experiment	ANFIS	Errors (%)
82	1200	350	0.09	3	0.34	0.35	− 2.86
83	1300	450	0.09	4	0.39	0.38	2.63
84	1400	350	0.1	3	0.35	0.34	2.86
85	1350	300	0.12	4	0.36	0.37	− 2.70
86	1700	450	0.06	2	0.53	0.52	1.92
87	1450	500	0.08	3	0.42	0.43	− 2.33
88	1600	400	0.09	3	0.38	0.39	− 2.56

Table 8 Comparative errors for the machining noise model

No.	S (RPM)	f (mm/min)	D (mm)	N	MN (dB)		
					Experiment	ANFIS	Errors (%)
82	1200	350	0.09	3	68.1	68.1	− 0.44
83	1300	450	0.09	4	76.9	76.9	0.52
84	1400	350	0.1	3	71.3	71.3	− 0.42
85	1350	300	0.12	4	75.7	75.7	0.53
86	1700	450	0.06	2	70.1	70.0	− 0.43
87	1450	500	0.08	3	74.7	74.9	0.56
88	1600	400	0.09	3	74.2	74.2	− 0.54

machining temperature in the burnishing region, which results in reductions in the strength and hardness of the workpiece. Lower energy consumed is required to process the material; hence, energy efficiency is enhanced. The similar impacts of the spindle speed and feed rate on the energy efficiency for the milling and turning processes can be found in the works of [26, 27].

Figure 13 b presents the influences of the burnishing depth and number of rollers on energy efficiency. It can be stated that the higher energy efficiency is found with an increased burnishing depth and/or the number of rollers. The phenomena can be explained as follows. Higher burnishing depth causes increased machining pressure, leading to greater resistance on the burnished surface. As a result, a higher burnishing power consumed is required to overcome resistance and compress material; hence, energy efficiency is increased. When the number of rollers increases, the distance between the burnishing traces decreases, leading to an increased burnishing pressure. Consequently, higher burnishing power is required to overcome greater resistance and compress the material; hence, energy efficiency is enhanced.

The impacts of burnishing parameters on the surface roughness are illustrated in Fig. 14.

Figure 14 a presents the impacts of the spindle speed and feed rate on the surface roughness. As a result, the roughness is firstly decreased when the spindle speed changes from 1000 to 1400 RPM, while further spindle speed causes an increased roughness. Additionally, a higher feed rate leads to increased roughness. The phenomena can be explained as follows. When the spindle speed increases, the temperature in the

Table 9 ANOVA results for the energy efficiency model

Source	Sum of squares	Mean square	F value	*p*-value	Remark	Contributions (%)
Model	595.61104	42.54365	33.12647	< 0.0001	Significant	
S	104.43147	104.43147	81.31519	< 0.0001	Significant	17.04
f	141.76431	141.76431	110.38427	< 0.0001	Significant	23.14
D	116.48361	116.48361	90.69955	< 0.0001	Significant	19.01
N	99.93413	99.93413	77.81335	< 0.0001	Significant	16.31
Sf	19.54567	19.54567	15.21917	0.0030	Significant	3.19
SD	5.89336	5.89336	4.58884	0.0984	Insignificant	0.96
SN	6.99355	6.99355	5.44550	0.0090	Significant	1.14
fD	3.30867	3.30867	2.57629	0.1062	Insignificant	0.54
fN	14.15376	14.15376	11.02077	0.0040	Significant	2.31
DN	9.50324	9.50324	7.39966	0.0060	Significant	1.55
S^2	21.23677	21.23677	16.53593	0.0020	Significant	3.47
f^2	27.02265	27.02265	21.04109	0.0009	Significant	4.41
D^2	19.68721	19.68721	15.32937	0.0029	Significant	3.21
N^2	22.77101	22.77101	17.73057	0.0024	Significant	3.72
Residual	14.12708	1.28428				
Total	609.73811					

R^2 = 0.9768; Adjusted R^2 = 0.9632; Predicted R^2 = 0.9586

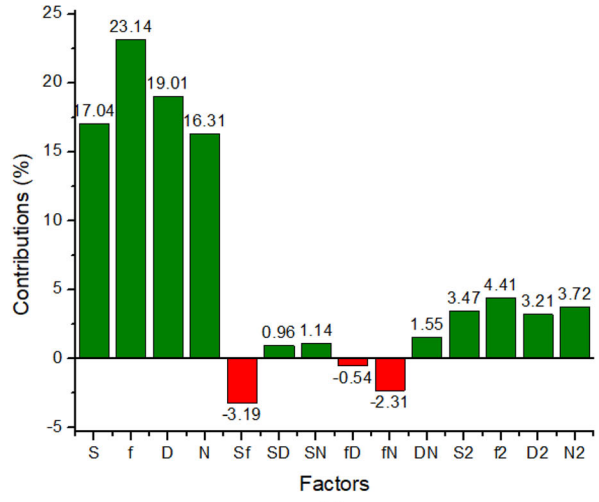

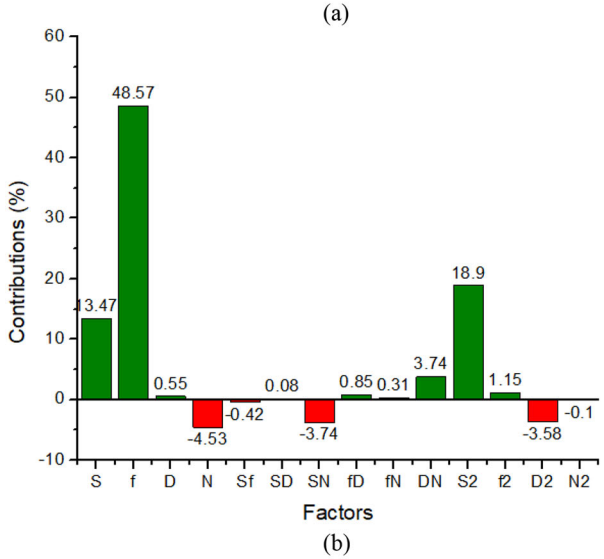

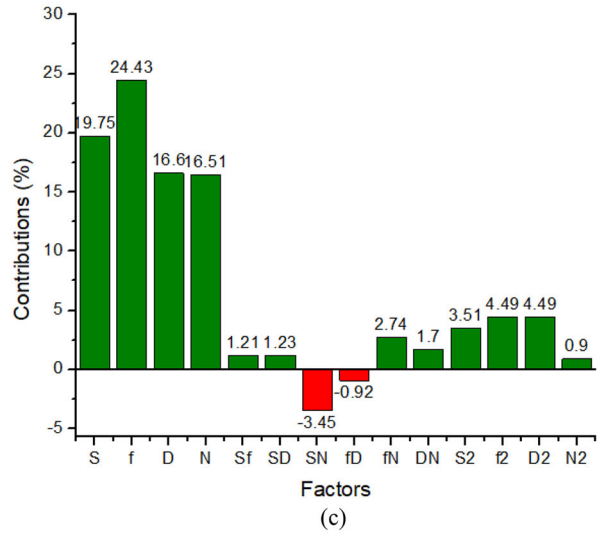

Fig. 12 Parametric contributions for burnishing performances. **a** For energy efficiency model. **b** For surface roughness model. **c** For machining noise model

burnishing region increases; hence, the workpiece hardness and strength are decreased. The material is easily compressed and the roughness is significantly reduced. Further spindle speed may lead the excessive machining temperature, the work-hardening behavior may occur on the burnished surface. The machined surface is hardly burnished; hence, a higher roughness is produced. A low feed rate results in a short distance between the successively burnishing traces, which causes a reduction in the burnished peaks; hence, lower roughness is produced. A higher feed results in a larger distance between the burnishing traces increases, which causes a higher roughness. Moreover, further feed rate may lead to excessive machining temperature, which causes the work-hardening behavior on the machined surface. The material is hardly compressed; hence, a higher roughness is produced. The influences of the feed rate and spindle speed on the surface roughness were similarly described in the works of [2, 3, 12, 13, 17, 18].

Figure 14 b presents the impacts of the burnishing depth and number of rollers on the surface roughness. As a result, a lower roughness is obtained with an increased burnishing depth and/or the number of rollers. The phenomena can be explained as follows. A low burnishing depth causes a reduction in the machining pressure and a small amount of material is compressed. A small degree of plastic deformation is produced, which causes a higher roughness. An increased burnishing depth leads to a higher machining pressure, which causes a larger degree of plastic deformation. A higher amount of the material is compressed and low surface roughness is produced. Additionally, an increment in the number of rollers causes higher burnishing pressure due to a reduction in the distance between the burnishing traces. The degree of plastic deformation increases and more material is burnished; hence, the surface roughness is decreased. A reduction in the surface roughness with an increased burnishing depth and/or the number of rollers can be found in the works of [8, 9, 14, 20].

The surface morphology produced at various process parameters is presented in Fig. 14. In this work, a scanning electron microscope labeled Nano Nova 450 is used to detect the surface morphology at different machining conditions. An increased feed rate causes higher roughness. The small grooves, cracks, and waviness are obtained at a low feed rate (Fig. 15a). Larger cracks, holes, and grooves are produced with an increased feed rate (Fig. 15b).

The influences of burnishing parameters on the machining noise are shown in Fig. 16.

Figure 16 a presents the impacts of the spindle speed and feed rate on the machining noise. As a result, a higher machining noise is found with an increment in the spindle speed and/or feed rate. An increased spindle speed causes higher momentum in the main spindle, which leads to an increased power consumed by the motor. A higher working load is then

Table 10 ANOVA results for the surface roughness model

Source	Sum of squares	Mean square	F value	*p*-value	Remark	Contributions (%)
Model	0.30191	0.02156	36.16966	< 0.0001	Significant	
S	0.03968	0.03968	66.54511	< 0.0001	Significant	13.47
f	0.14301	0.14301	239.86150	< 0.0001	Significant	48.57
D	0.00163	0.00163	2.73952	0.1261	Insignificant	0.55
N	0.01333	0.01333	22.36341	0.0006	Significant	4.53
Sf	0.00123	0.00123	2.05464	0.1795	Insignificant	0.42
SD	0.00023	0.00023	0.37738	0.5515	Insignificant	0.08
SN	0.01103	0.01103	18.49174	0.0013	Significant	3.74
fD	0.00250	0.00250	4.19314	0.0652	Insignificant	0.85
fN	0.00090	0.00090	1.50953	0.2448	Insignificant	0.31
DN	0.01103	0.01103	18.49174	0.0013	Significant	3.74
S^2	0.05564	0.05564	93.31766	< 0.0001	Significant	18.90
f^2	0.00340	0.00340	5.70394	0.0360	Significant	1.15
D^2	0.01055	0.01055	17.69250	0.0015	Significant	3.58
N^2	0.00030	0.00030	0.50826	0.4907	Insignificant	0.10
Residual	0.00656	0.00060				
Total	0.30847					

R^2 = 0.9787; Adjusted R^2 = 0.9676; Predicted R^2 = 0.9612

produced; hence, bigger machining noise is generated. An increased feed rate requires higher power consumption in the drive system to satisfy the setting value, which causes an increased noise emission. Moreover, a higher feed rate may cause excessive temperature in the burnishing region, which results in the work-hardening behavior on the burnished surface. The strength and hardness of the burnishing specimen are then increased, which causes greater resistance on the burnished surface. The workpiece hardly is processed, as compared to the initial state. As a result, a higher power

Table 11 ANOVA results for the machining noise model

Source	Sum of squares	Mean square	F value	*p*-value	Remark	Contributions (%)
Model	1790.77904	127.91279	28.74591	< 0.0001	Significant	
S	352.76655	352.76655	79.27748	< 0.0001	Significant	19.75
f	436.22535	436.22535	98.03324	< 0.0001	Significant	24.43
D	296.49036	296.49036	66.63049	< 0.0001	Significant	16.60
N	294.84726	294.84726	66.26124	< 0.0001	Significant	16.51
Sf	21.58891	21.58891	4.85169	0.0400	Significant	1.21
SD	21.97468	21.97468	4.93839	0.0400	Significant	1.23
SN	61.61627	61.61627	13.84707	0.0012	Significant	3.45
fD	16.43101	16.43101	3.69255	0.0700	Insignificant	0.92
fN	48.91439	48.91439	10.99257	0.0010	Significant	2.74
DN	30.35986	30.35986	6.82279	0.0300	Significant	1.70
S^2	62.71286	62.71286	14.09351	0.0011	Significant	3.51
f^2	80.18867	80.18867	18.02086	0.0009	Significant	4.49
D^2	80.18867	80.18867	18.02086	0.0009	Significant	4.49
N^2	16.06345	16.06345	3.60995	0.0700	Insignificant	0.90
Residual	48.94750	4.44977				
Total	1839.726538					

R^2 = 0.9734; Adjusted R^2 = 0.9652; Predicted R^2 = 0.9576

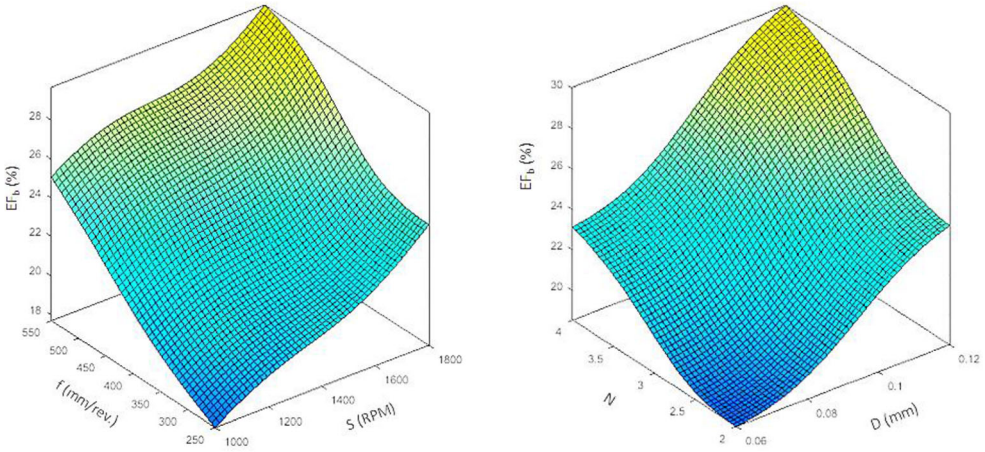

(a) (b)

Fig. 13 The influences of the burnishing parameters on the EF_b. **a** Energy efficiency versus the spindle speed and feed rate. **b** Energy efficiency versus the burnishing depth and number of rollers

consumed of the feed drive system is required to overcome resistance and burnish material; hence, the intensity of the machining noise is increased.

Figure 16 b presents the impacts of the burnishing depth and number of rollers on the machining noise. It can be stated that higher machining noise is produced with an increased burnishing depth and/or the number of rollers. An increased burnishing depth causes a higher degree of plastic deformation and more material is processed. Greater resistance is produced and a higher burnishing load is required; hence, the intensity of the machining noise increases. An increment in the rollers causes a reduction in the peripheral distance between the rollers. In other words, higher rollers lead to an increased frequency of engagement; hence, a higher degree of plastic deformation is obtained. More material is compressed and burnished, which requires a higher burnishing load. Consequently, the noise emission increases with higher rollers.

4.4 Optimization results using ANFIS-NOPSO

Table 12 lists the entropy value, dispersion value, and weight for each criterion. As a result, the weight values of the energy efficiency, surface roughness, and machining noise are 0.27, 0.39, and 0.34, respectively.

The ANFIS models of energy efficiency, surface roughness, and machining noise are employed to select the optimal factors. The Pareto fronts generated by NSPSO are shown in Fig. 17.

Based on the optimization requirement, solution no. 322 is selected as the optimal point. As a result, the optimum values of the spindle speed, feed rate, burnishing depth, and the number of rollers are 1645 RPM, 260 mm/min, 0.08 mm, and 4, respectively. The reductions in the surface roughness and machining noise are 25.0% and 2.23%, respectively, while the energy efficiency is enhanced by 6.25%, as compared to the initial values (Table 13).

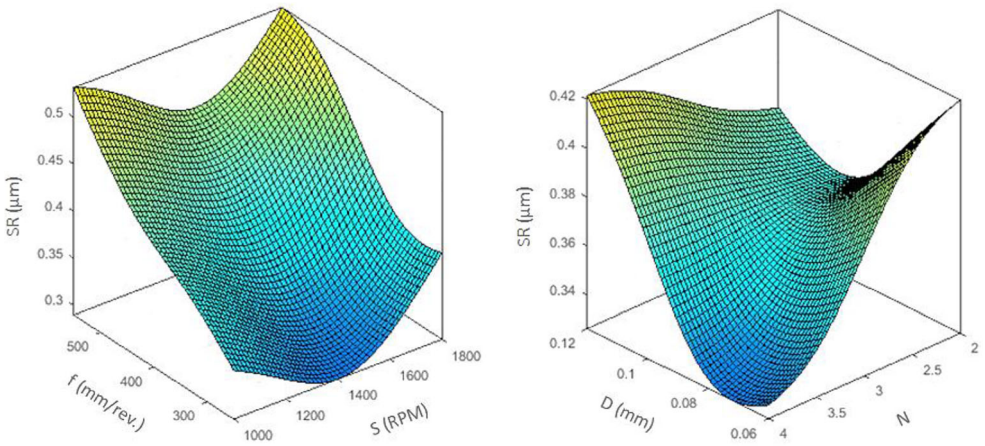

(a) (b)

Fig. 14 The influences of the burnishing parameters on the SR. **a** Surface roughness versus the spindle speed and feed rate. **b** Surface roughness versus the burnishing depth and number of rollers

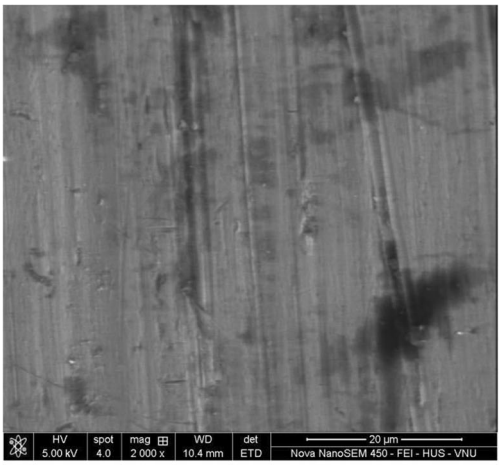

(a)

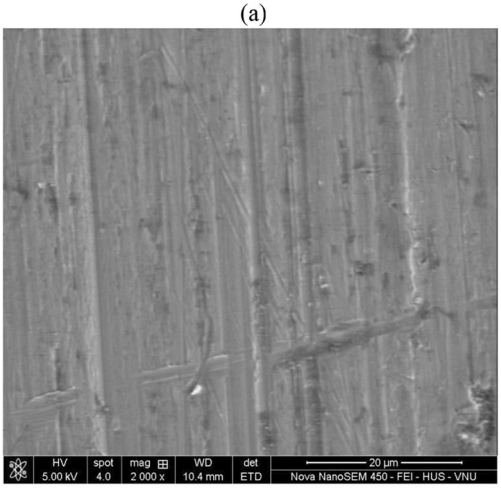

(b)

Fig. 15 Surface morphology at various burnishing trails: **a** At process parameters: S = 1600 RPM, f = 250 mm/rev., D = 0.06 mm, N = 4. **b** At process parameters: S = 1600 RPM, f = 550 mm/rev., D = 0.08 mm., N = 4

4.5 Optimization results using RSM-DA

To evaluate the effectiveness of the ANFIS-NOPSO, the RSM and DA are applied to develop the predictive models of the burnishing responses and select the optimal factors. The R^2-values of the RSM models of the EF_b, SR, and MN are 0.9532, 0.9546, and 0.9528, respectively. The visualizations of the RSM graphs for energy efficiency, surface roughness, and machining noise are depicted in Figs. 18, 19, and 20, respectively.

The mathematical models of the EF_b, SR, and MN are expressed as:

$$EF_b = 7.09667 - 0.00261S + 0.02134f - 37.10417D - 1.50917N - 0.000007Sf + 0.00045SN - 0.00206fN + 8.0625DN + 0.0000034S^2 + 0.000022f^2 + 556.77083D^2 + 0.57958N^2 \quad (26)$$

$$SR = 1.21083 - 0.00079S - 0.00024f - 10.5D + 0.06N - 0.00013SN + 1.125DN + 0.00000044S^2 + 0.00000079f^2 + 33.85417D^2 \quad (27)$$

$$MN = 33.95417 - 0.00043S - 0.00596f + 189.375D + 2.83333N + 0.000004Sf + 0.02375SD - 0.002SN + 0.00363fN + 13.125DN + 0.0000051S^2 + 0.000034f^2 - 658.85417D^2 \quad (28)$$

The DA is employed to select the optimal outcomes of process parameters and responses with the aid of the developed formulas. The ramp graphs showing optimal values are shown in Fig. 21. As a result, the optimum values generated by the RSM-DA of the spindle speed, feed rate, burnishing depth, and the number of rollers are 1400 RPM, 250 mm/min, 0.09 mm, and 4, respectively (Table 14). The reduction in the surface roughness is 22.22%, while the energy efficiency is enhanced by 4.424%. Unfortunately, the machining noise is decreased by 0.14%, as compared to the initial value.

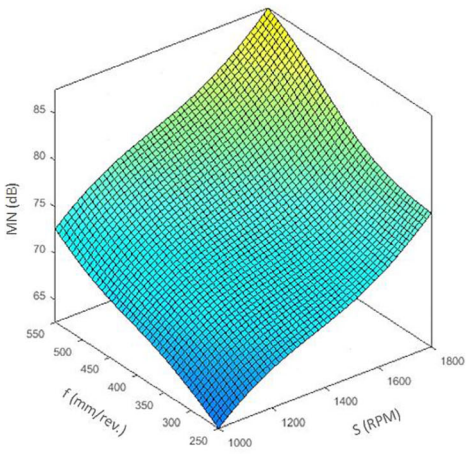

(a)

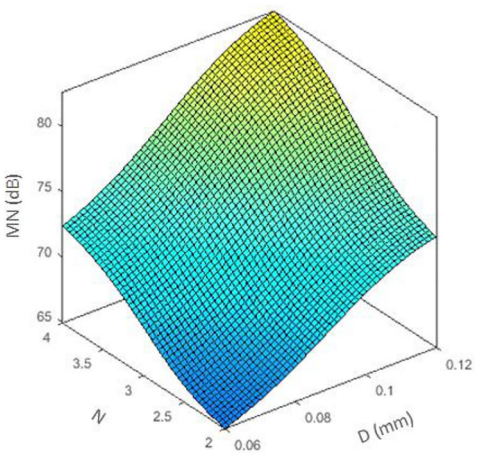

(b)

Fig. 16 The influences of the burnishing parameters on the MN. **a** Machining noise versus the spindle speed and feed rate. **b** Machining noise versus the burnishing depth and number of rollers

Table 12 Entropy value, dispersion value, and weight for each criterion

Criteria	EF_b	SR	MN
Entropy value	0.963451	0.947827	0.95507
Dispersion value	0.036549	0.052173	0.04493
Weight	0.27	0.39	0.34

4.6 Comparisons of optimization results

As shown in ANOVA results, the R^2 values of the ANFIS models for the energy efficiency, surface roughness, and machining noise are 0.9768, 0.9787, and 0.9734, respectively. The R^2 values of the RSM models for the energy efficiency, surface roughness, and machining noise are 00.9532, 0.9546, and 0.9528, respectively. It can be stated that the R^2 values produced by RSM models are lower than the ANFIS models. In other words, the ANFIS models are more adequate than the RSM approach. As depicted in Figs. 13, 14, and 16, the ANFIS models are effectively applied to render the highly nonlinear relationships between the process parameters and burnishing responses.

As given in Table 13, the improvements in the energy efficiency, surface roughness, and machining noise are

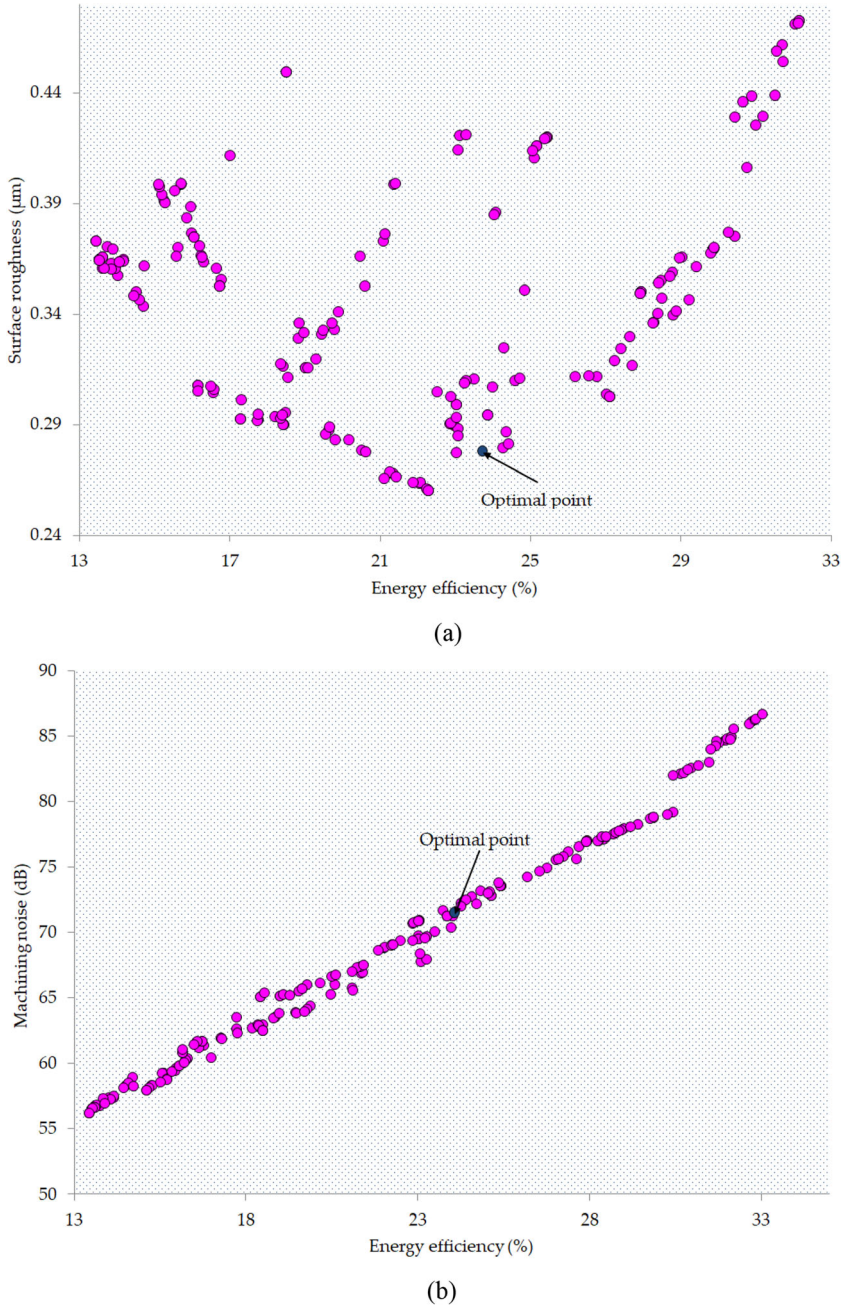

Fig. 17 Pareto graphs. **a** Energy efficiency versus surface roughness. **b** Energy efficiency versus machining noise

Table 13 Optimization results using the ANFIS-PSO

Method	Optimization parameters				Responses		
	S (RPM)	f (mm/min)	D (mm)	N	EF_b (%)	SR (μm)	MN (dB)
Used values	1400	400	0.09	3	22.65	0.36	71.7
Optimal results	1645	260	0.08	4	24.23	0.27	70.1
Improvement (%)					6.98	25.00	2.23

6.98%, 25.00%, and 2.23%, respectively at the optimal solution produced by the ANFIS-NOPSO. As shown in Table 14, the improvements in the surface roughness and energy efficiency are 22.22% and 4.42%, respectively, while the machining noise is decreased by 0.14% at the optimal solution produced by the RSM-DA. Consequently, it can be stated that the ANFIS-NOPSO provides better optimization results than the RSM-DA while dealing with multi-objective optimization in the internal burnishing process.

4.7 Evaluation of the production costs

The cost of energy consumed in the burnishing operation (C_{energy}) is calculated as:

$$C_{\text{energy}} = c_e E_{\text{total}} \tag{29}$$

where c_e, the energy cost per unit energy (VND/kWh); E_{total}, the total energy consumed (kJ).

The cost of the burnishing tool (C_{tool}) is computed as:

$$C_{\text{tool}} = c_c \frac{t_b}{T} \tag{30}$$

where c_c, the cost to fabricate the burnishing tool (VND/piece); T_T, the tool life of the roller (s).

The labor cost (C_{labor}) is computed as:

$$C_{\text{labor}} = c_{\text{labor}}(t_o + t_{st} + t_{\text{air}} + t_{ch} + t_b) \tag{31}$$

where t_o, t_{st}, t_{air}, and t_{ch} denotes the start-up, setup, air-burnishing, tool change, and burnishing time, respectively. c_{labor} presents the labor cost (VND/s).

The cost of the tool change ($C_{tool\ change}$) is computed as:

$$C_{\text{toolchange}} = c_{\text{labor}} t_{ch} \frac{t_b}{T_T} \tag{32}$$

The cost of the lubricant used (C_{fluid}) is calculated as:

$$C_{fluid} = \frac{(c_{fp} + c_{fd})(t_o + t_{st} + t_{\text{air}} + t_{ch} + t_b)V_a}{T_{use}} \tag{33}$$

where V_a, the volume consumed of the lubricant; t_{use}, the time of the lubricant replacement (month); c_{fp}, the cost for the lubricant preparation (VND/l); c_{fd}, the cost for the lubricant disposal (VND/l).

The cost of the machine degradation and remanufacturing ($C_{machine}$) is computed as:

$$C_{machine} = \frac{(c_{md} + c_{mr})(t_o + t_{st} + t_{\text{air}} + t_{ch} + t_b)}{T_m} \tag{34}$$

where: c_{md}, the cost of the machine degradation (VND); c_{mr}, the cost of the machine remanufacturing (VND). T_m, the service life of the machine used (years).

The cost of the machining noise (C_{noise}) is computed as:

$$C_{machine} = \frac{c_n(t_o + t_{st} + t_{\text{air}} + t_{ch} + t_b)}{8 \times 3600 \times 30} \tag{35}$$

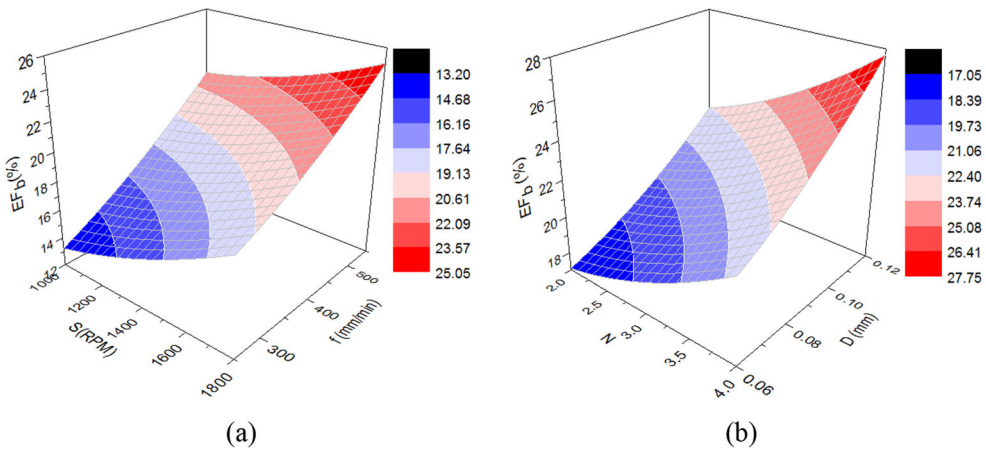

Fig. 18 The RSM graphs for the EF_b. **a** EF_b versus S and f. **b** EF_b versus D and N

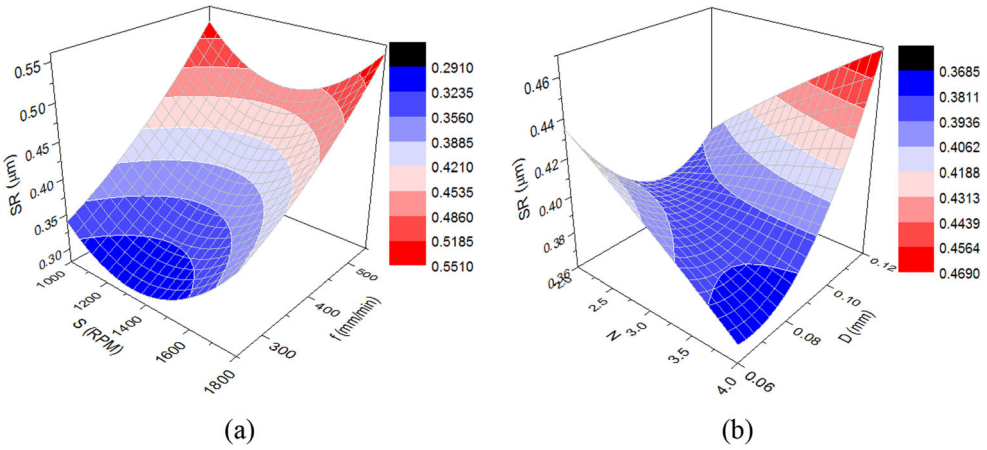

Fig. 19 The RSM graphs for the SR. **a** SR versus S and f. **b** SR versus D and N

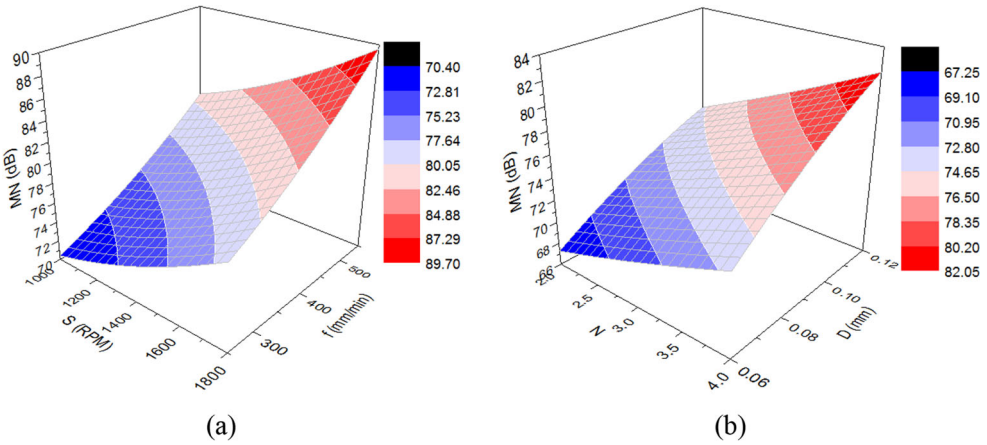

Fig. 20 The RSM graphs for the MN. **a** MN versus S and f. **b** MN versus D and N

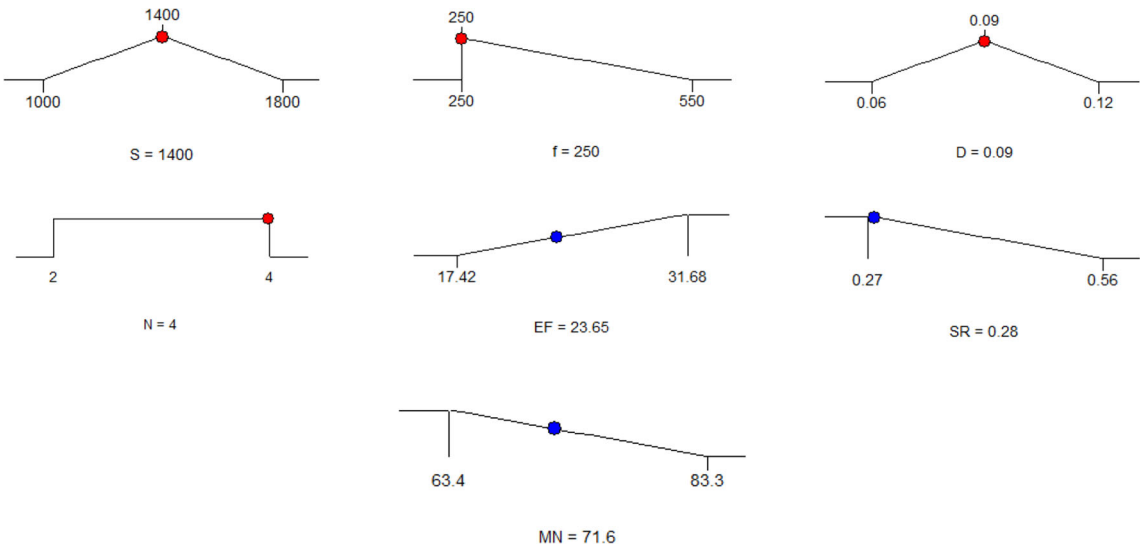

Fig. 21 Optimal parameters in the Ramps generated by DA

Table 14 Optimization results using the RSM-DA

Method	Optimization parameters				Responses		
	S (RPM)	f (mm/min)	D (mm)	N	EF_b (%)	SR (μm)	MN (dB)
Used values	1400	400	0.09	3	22.65	0.36	71.7
Optimal results	1400	250	0.09	4	23.65	0.28	71.6
Improvement (%)					− 4.42	22.22	0.14

where c_n, the noise tax per month (VND).

The comprehensive model for the cost of the burnishing operation (C_{total}) is expressed as:

$$C_{total} = C_{energy} + C_{labor} + C_{toolchange} + C_{fluid} + C_{machine} + C_{noise} \quad (36)$$

Table 15 presents the coefficients of the cost model. As a result, the total cost of the burnishing process is decreased by 6.2% at the optimal solution (Table 16).

5 Conclusions

In the current investigation, a machining-based optimization of the internal roller burnishing operation has been executed to boost energy efficiency and decrease the surface roughness and machining noise. Burnishing parameters are the spindle speed, feed rate, burnishing depth, and the number of rollers. The ANFIS approach was applied to develop comprehensive models of the technical performances regarding process parameters. The entropy method was employed to calculate the weights of the burnishing objectives. The dominated sorting particle swarm optimization was utilized to find optimal outcomes. The obtained findings can be listed as bellows:

1. The highest values of burnishing parameters can be applied to enhance the energy efficiency, while the lowest levels of the inputs are commended to decrease the machining noise. Higher burnishing depth and/or the number of rollers can be employed to decrease the surface roughness, while a low feed rate leads to a reduction in the roughness. The middle value of the spindle speed is applied to obtain a smooth surface.
2. ANOVA results indicated that the ANFIS models of energy efficiency, surface roughness, and machining noise are significant. These models can be applied to forecast the burnishing responses in industrial applications with acceptable precision. Moreover, the proposed models can be directly employed for the internal roller burnishing operation of the hardened SCr440 steel without expensive experimental costs and efforts.
3. As shown in the optimal setting generated by NSPSO, the optimal values of the spindle speed, feed rate, burnishing depth, and the number of rollers are 1645 RPM, 260 mm/min, 0.08 mm, and 4, respectively. The energy efficiency is improved by 6.98%, while the surface roughness and machining noise are decreased by 25.00% and 2.23%, respectively. The total cost of the burnishing process is decreased by 6.2% at the optimal point.
4. The proposed approach using the ANFIS, entropy weight, and NSPSO can be used to model the comprehensive responses and to effectively select the optimal solution, as compared to the trial method and operator experience. This optimizing technique is powerful and can be applied to different burnishing operations. Moreover, the ANFIS-

Table 15 Experimental coefficients for the cost models

c_e	c_c	T_T	c_{labor}	P_o	P_{st}	P_{air}
VND/kWh	VND/piece	s	VND/s	kW	kW	kW
1736	460762	2100	1397.90	0.42	0.58	0.76
t_o	t_{st}	t_{air}	t_{ch}	V_a		
s	s	s	s	l		
5	5	8	15	200		
T_{use}	c_{fp}	c_{fd}	c_{md}	c_{mr}	T_m	c_n
Month	VND/l	VND/l	VND	VND	year	VND/h
6	3535.26	10605.79	989874175.64	395949670.26	14	64341.82

Table 16 Comparative values of the total cost

Method	Optimization parameters				Response
	S (RPM)	f (mm/min)	D (mm)	N	Total cost (VND)
Initial values	1400	400	0.09	2	102717.81
Optimal results	1645	260	0.08	4	96391.55
Reduction (%)	–	–	–	–	6.2

NOPSO can provide better optimization results than the RSM-DA.

5. Practically, the energy consumption for the burnishing tool and fluid has negative impacts on the environment and machining costs. Therefore, a comprehensive approach considering more sustainable performances can be addressed in the next investigation.

Nomenclature *AL (μm),* Depth of the affected layers; *ANFIS,* Adaptive neuro-fuzzy inference system; *SR (μm),* Surface roughness; *BE (kJ),* Burnishing energy; *BS (mm),* Bore size; *D (mm),* Burnishing depth; *EC (kJ),* Energy consumed; EF_b *(%),* Energy efficiency; *f (mm/min),* Feed rate; *F (N),* Burnishing force; *L,* Lubricant; *MH (VH),* Micro-hardness; *MN (dB),* Machining noise; *MQL,* Minimum quantity lubrication; *N,* Number of rollers; *NOPSO,* Non-dominated sorting particle swarm optimization; *NP,* Number of passes; *OV,* Ovality; *PF,* Power factor; *PI (μm),* Profile irregularities; *RS (MPa),* Residual stress; *RSM,* Response surface method; *RW (mm),* Roller width; R_y *(μm),* Maximum height roughness; *S (RPM),* Spindle speed; *SH (HRC),* Surface hardness; *SO (mm),* Step-over; *V (m/min),* Burnishing speed; *VH (VH),* Vicker hardness

Author contribution Conceptualization, T.-T.N. and M.T.L.; methodology, T.-T.N. and M.T.L.; software, T.-T.N. and M.T.L.; validation, T.-T.N. and M.T.L.; data curation, T.-T.N.; writing—original draft preparation, T.-T.N. and M.T.L.; writing—review and editing, T.-T.N. and M.T.L.; All authors have read and agreed to the published version of the manuscript.

Funding This research is funded by Vietnam National Foundation for Science and Technology Development (NAFOSTED) under grant number 107.04-2020.02.

Data availability All data and materials have been included on the manuscript.

Declarations

Ethics approval All materials included in the manuscript are our own and do not require any copyright permission from the third party.

Consent to participate All authors have participated in the manuscript preparation.

Consent for publication All authors have agreed to transfer all materials included in the manuscript to the published if accepted.

Competing interests The authors declare no competing interests.

References

1. Rotella G, Rinaldi S, Filice L (2020) Roller burnishing of Ti6Al4V under different cooling/lubrication conditions and tool design: effects on surface integrity. Int J Adv Manuf Technol 106:431–440
2. Cobanoglu T, Ozturk S (2015) Effect of burnishing parameters on the surface quality and hardness. P I Mech Eng B-J Eng 229:286–294
3. Gharbi F, Sghaier S, Morel F (2015) Experimental investigation of the effect of burnishing force on service properties of AISI 1010 steel plates. J Mater Eng Perform 24:721–725
4. Banh QN, Shiou FJ (2016) Determination of optimal small ball-burnishing parameters for both surface roughness and superficial hardness improvement of STAVAX. Arab J Sci Eng 41:639–652
5. Yuan XL, Sun YW, Gao LS, Jiang SL (2016) Effect of roller burnishing process parameters on the surface roughness and microhardness for TA2 alloy. Int J Adv Manuf Technol 85:1373–1383
6. Amdouni H, Bouzaiene H, Montagne A, Nasri M, Iost A (2017) Modeling and optimization of a ball-burnished aluminum alloy flat surface with a crossed strategy based on response surface methodology. Int J Adv Manuf Technol 88:801–814
7. Amdouni H, Bouzaiene H, Montagne A, Nasri M, Iost A (2017) Experimental study of a six new ball-burnishing strategies effects on the Al-alloy flat surfaces integrity enhancement. Int J Adv Manuf Technol 90:2271–2282
8. John MRS, Banerjee N, Shrivastava K, Vinayagam BK (2017) Optimization of roller burnishing process on EN-9 grade alloy steel using response surface methodology. J Braz Soc Mech Sci Eng 39:3089–3101
9. Stalin John MR, Balaji B, Vinayagam BK (2017) Optimisation of internal roller burnishing process in CNC machining center using response surface methodology. J Braz Soc Mech Sci Eng 39:4045–4057
10. Teimouri R, Amini S, Bami AB (2018) Evaluation of optimized surface properties and residual stress in ultrasonic assisted ball burnishing of AA6061-T6. Measurement. 116:129–139
11. Kovácsac ZF, Viharos ZJ, Kodácsy J (2018) Determination of the working gap and optimal machining parameters for magnetic assisted ball burnishing. Measurement. 118:172–180
12. Nguyen TT, Le XB (2018) Optimization of interior roller burnishing process for improving surface quality. Mater Manuf Process 33:1233–1241
13. Nguyen TT, Le XB (2019) Optimization of roller burnishing process using Kriging model to improve surface properties. P I Mech Eng B-J Eng 233:2264–2282
14. Sachin B, Narendranath S, Chakradhar D (2019) Selection of optimal process parameters in sustainable diamond burnishing of 17-4 PH stainless steel. J Braz Soc Mech Sci Eng 41:219
15. Sachin B, Narendranath S, Chakradhar D (2019) Enhancement of surface integrity by cryogenic diamond burnishing toward the improved functional performance of the components. J Braz Soc Mech Sci Eng 41:396
16. Teimouri R, Amini S (2019) A comprehensive optimization of ultrasonic burnishing process regarding energy efficiency and workpiece quality. Surf Coating Tech 375:229–242
17. Nguyen TT, Cao LH, Dang XP, Nguyen TA, Trinh QH (2019) Multi-objective optimization of the flat burnishing process for energy efficiency and surface characteristics. Mater Manuf Process 34:1888–1901
18. Nguyen TT, Cao LH, Nguyen TA, Dang XP (2019) Multi-response optimization of the roller burnishing process in terms of energy consumption and product quality. J Clean Prod 245:119328
19. Nguyen TT, Le CH (2020) Optimization of compressed air assisted-turning-burnishing process for improving machining

quality, energy reduction and cost-effectiveness. P I Mech Eng B-J Eng https://doi.org/10.1177/0954405420976661
20. Duncheva GV, Maximov JT, Dunchev VP, Anchev AP, Atanasov TP, Capek J (2020) Single toroidal roller burnishing of 2024-T3 Al alloy implemented as mixed burnishing process. Int J Adv Manuf Technol 111:3559–3570
21. Okada M, Terada S, Shinya M, Sasaki T, Kataoka Y, Kihara T, Miura T, Otsu M (2020) Surface finishing and enhancement of Ni-based alloy using sliding burnishing with active rotary tool. Int J Adv Manuf Technol 107:4661–4676
22. Asadi R, Yeganefar A, Niknam SA (2019) Optimization and prediction of surface quality and cutting forces in the milling of aluminum alloys using ANFIS and interval type 2 neuro fuzzy network coupled with population-based meta-heuristic learning methods. Int J Adv Manuf Technol 105:2271–2287
23. Yang B, Liu Z (2020) Thermal error modeling by integrating GWO and ANFIS algorithms for the gear hobbing machine. Int J Adv Manuf Technol 109:2441–2456
24. Shaomin L, Deyuan Z, Daxi G, Zhenyu S, Hui T (2019) Modeling and drilling parameters optimization on burr height using harmony search algorithm in low-frequency vibration-assisted drilling. Int J Adv Manuf Technol 101:2313–2325
25. Shaomin L, Deyuan Z, Zhenyu S, Hui T (2020) Information feedback self-adaptive harmony search algorithm for the bovine cortical bone vibration-assisted drilling optimization. Measurement 149: 107020
26. Nguyen TT, Nguyen TA, Trinh QH (2020) Optimization of milling parameters for energy savings and surface quality. Arab J Sci Eng 45:9111–9125
27. Nguyen TT, Duong QD, Mia M (2020) Sustainability-based optimization of the rotary turning of the hardened steel. Metals 10:939

Publisher's note Springer Nature remains neutral with regard to jurisdictional claims in published maps and institutional affiliations.